JCI The Journal of Clinical Investigation

Mitochondrial- and NOX4-dependent antioxidant defence mitigates progression to non-alcoholic steatohepatitis in obesity

Spencer Greatorex, … , Matthew J. Watt, Tony Tiganis

J Clin Invest. 2023. https://doi.org/10.1172/JCI162533.

Research In-Press Preview Hepatology Metabolism

Graphical abstract

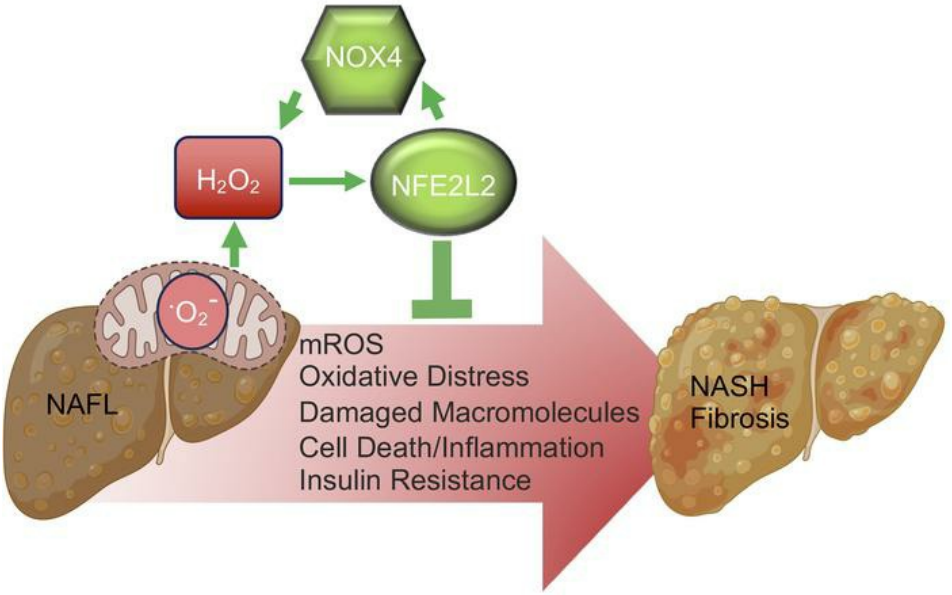

Mitochondrial- and NOX4-dependent antioxidant defense mitigates progression to non-alcoholic steatohepatitis in obesity

Spencer Greatorex [1, 2 #], Supreet Kaur [1, 2 #], Chrysovalantou E. Xirouchaki [1, 2 #], Pei K., Goh [1, 2], Florian Wiede [1, 2], Amanda J. Genders [1, 2], Melanie Tran [2], YaoYao Jia [1, 2], Arthe Raajendiran [1, 2], Wendy A. Brown [3], Catriona A. McLean [4], Junichi Sadoshima [5], Matthew J. Watt [6] and Tony Tiganis [1, 2]

[1] Monash Biomedicine Discovery Institute, Monash University, Clayton, Victoria 3800, Australia.
[2] Department of Biochemistry and Molecular Biology, Monash University, Clayton, Victoria 3800, Australia.
[3] Monash University Department of Surgery, Alfred Hospital, Melbourne, Victoria, 3004, Australia
[4]Anatomical Pathology, Alfred Hospital, Prahran, Victoria 3004, Australia
[5] Department of Cell Biology and Molecular Medicine, Cardiovascular Research Institute, Rutgers New Jersey Medical School, Newark, New Jersey, USA.
[6] Department of Anatomy and Physiology, University of Melbourne, Victoria 3010, Australia

# contributed equally

Correspondence: Tony Tiganis
23 Innovation Walk
Monash University
Victoria 3800
Australia
+61 3 9902 9332
Tony.Tiganis@monash.edu

The authors declare no competing interests.

ABSTRACT

Non-alcoholic fatty liver disease (NAFLD) is prevalent in the majority of obese individuals, but in a subset, this progresses to non-alcoholic steatohepatitis (NASH) and fibrosis. The mechanisms that prevent NASH and fibrosis in the majority of NAFLD patients remain unclear. Here we report that NAD(P)H oxidase (NOX)-4 and nuclear factor erythroid 2-related factor 2 (NFE2L2) were elevated in hepatocytes early in disease progression to prevent NASH/fibrosis. Mitochondrial-derived reactive oxygen species (ROS) activated NFE2L2 to induce the expression of NOX4, which in turn generated H_2O_2 to exacerbate the NFE2L2 antioxidant defense response. The deletion or inhibition of NOX4 in hepatocytes decreased ROS and attenuated antioxidant defense to promote mitochondrial oxidative stress, damage proteins and lipids, diminish insulin signalling and promote cell death upon oxidant challenge. Hepatocyte NOX4 deletion in high fat fed obese mice, which otherwise develop steatosis, but not NASH, resulted in hepatic oxidative damage, inflammation and T cell recruitment to drive NASH and fibrosis, whereas NOX4 overexpression tempered the development of NASH/fibrosis in mice fed a NASH-promoting diet. Thus, mitochondrial- and NOX4-derived ROS function in concert to drive a NFE2L2 antioxidant defense response to attenuate oxidative liver damage and the progression to NASH/fibrosis in obesity.

INTRODUCTION

NAFLD has reached epidemic proportions, affecting 20-30% of the world's population (1, 2). Although there are strong genetic determinants for disease onset and progression, the prevalence of NAFLD can be attributed predominantly to the entrenched and growing obesity and diabetes epidemics (1-3). NAFLD encompasses disorders ranging from simple steatosis, or non-alcoholic fatty liver (NAFL), to NASH evident in 20-30% of NAFLD patients and characterised by chronic lipid accumulation, liver damage and lobular/portal inflammation involving the recruitment and activation of immune cells, especially T cells. The liver damage and inflammation elicit reparative processes that result in fibrosis (1). Ultimately, persistent reparative responses can lead to severe fibrosis or cirrhosis and end-stage liver disease, or even hepatocellular carcinoma (HCC) (1, 4). NASH is currently the second leading cause for liver transplantation, the fastest growing cause for HCC and a major contributor to cardiovascular disease (1, 4, 5).

It is well established that the severity of steatosis can predict progression to NASH, as well as the risk for cirrhosis (1, 6). Genetic polymorphisms in *PNPLA3* that increase the risk for steatosis also increase the risk for NASH (1, 6). Steatosis occurs as a consequence of increased lipogenesis, increased uptake of dietary fatty acids and carbohydrates, and as a result of adipose tissue insulin resistance and the flux of free fatty acids to the liver (1, 6). However, the accumulation of lipids alone is not sufficient to drive progression to NASH/fibrosis. Indeed, the overexpression of DGAT2 in mice, or the deletion of ATGL in hepatocytes both increase steatosis without promoting inflammation, a key feature of NASH (7, 8). Chronic lipid accumulation in NAFL can increase mitochondrial β-oxidation and respiration (6, 9-11). The increased fatty acid oxidation and the excess supply of reduced substrates to the electron transport chain (ETC) is thought to result in increased electron leakage to generate superoxide ($O2^{\bullet -}$) (9, 12), but mitochondrial abnormalities or functional changes in the ETC may also

contribute (9, 10, 13-15). Genetic and pharmacological studies in rodents point toward mitochondrial oxidative stress not only promoting insulin resistance, a key driver of NAFLD (15-21), but also NASH and fibrosis (9, 20, 21). Indeed, a common polymorphism in the gene encoding mitochondrial-targeted superoxide dismutase (SOD)-2 that converts $O2^{\bullet-}$ into H_2O_2, diminishes SOD-2 function and is associated with more advanced fibrosis in NASH (22). However, several other processes including inflammation, ER stress, and increased NOX expression might also contribute to reactive oxygen species (ROS) generation (9, 23-26). In particular, the expression of NOX4, which can generate both $O2^{\bullet-}$ and H_2O_2 (27), is increased in the livers of patients with NAFLD and its deletion in hepatocytes has been shown to attenuate NASH/fibrosis in mice fed a NASH-promoting diet (24). $O2^{\bullet-}$ can react with nitric oxide to generate toxic peroxynitrite, or promote the conversion of H_2O_2 into highly reactive hydroxyl radicals to damage proteins, lipids and DNA (9). Increased ROS and the oxidative damage of macromolecules have been noted in the livers of rodents or patients with NAFLD (10, 28-31), and such oxidative damage can promote cell death and elicit reparative and inflammatory responses that result in fibrosis (9). Moreover, oxidative stress in NAFLD can result in the oxidative inactivation of protein tyrosine phosphatases in hepatocytes to promote tyrosine phosphorylation-dependent signaling including STAT-1 signaling to facilitate T cell recruitment, inflammation and the progression to NASH/fibrosis (32).

Given the potential for lipid accumulation to drive oxidative stress, it is perplexing why the majority of NAFLD patients don't progress to NASH/fibrosis. One possibility is that adaptive mechanisms temper the oxidative damage that may otherwise occur along the NAFLD continuum. One such mechanism may involve NFE2L2, a transcription factor that binds to antioxidant response elements (AREs) in the promoter regions of (33). Although NFE2L2 is normally targeted for degradation by the KEAP-1/Cullin-3 E3 ligase complex, ROS oxidise Cys residues on KEAP-1 to facilitate the release and translocation of NFE2L2 to the nucleus

to drive the expression of >200 endogenous antioxidant and xenobiotic detoxifying enzymes (33). Interesting, the *NFE2L2* gene contains AREs within its promoter region so that the NFE2L2 protein can drive its own transcription to amplify NFE2L2's effects (34). Genetic studies in mice have yielded conflicting evidence as to the roles of NFE2L2 and KEAP-1 in NAFLD. (35-40). We report that hepatic NFE2L2 target genes are elevated in NAFLD and that this serves to attenuate the progression to NASH and fibrosis. We show that the induction/activation of NFE2L2 is reliant on ROS generated by both mitochondria and NOX4 and that *Nox4* deletion in hepatocytes is sufficient to abrogate antioxidant defense response to promote oxidative lipid and protein damage, cell death, inflammation and the transition to NASH/fibrosis in obesity.

RESULTS

NFE2L2 redox signatures in NAFLD

To assess redox balance in NAFLD, we first took advantage of a publicly available RNAseq dataset (41) to assess the expression of redox genes in liver biopsies from lean or overweight subjects (BMI 25.9±5.8) without steatosis [NAFLD Activity Score (NAS)=0-1], overweight or obese subjects (BMI 33.9±5.8) with NAFL and mild lobular inflammation (NAS=1-4), NASH (NAS=1-6) with mild fibrosis (fibrosis score=1), or NASH (NAS=2-6) with significant or advanced fibrosis (fibrosis score ≥2) (**Table 1**). The expression of genes targeted by NFE2L2 increased in NAFL and NASH with mild fibrosis, but decreased in NASH with more advanced fibrosis (**Fig. 1a**). In particular, *NQO1*, which encodes the superoxide scavenger NAD(P)H dehydrogenase (quinone 1), *SOD2*, which converts $O2^{\bullet -}$ into H_2O_2 and catalase (*CAT*), which eliminates H_2O_2, were increased with NAFL and NASH with mild fibrosis, but tended to decline in NASH with significant/advanced fibrosis. Interestingly, the expression of *NOX4*, which has two NFE2L2-binding AREs in its promoter (42), also increased in NAFL and NASH with mild fibrosis but declined in NASH with significant/advanced fibrosis (**Fig. 1a**). Consistent with this, *NFE2L2*, *NQO1*, *SOD2*, *CAT* and *NOX4* mRNA levels, as assessed by quantitative real time PCR (qPCR) (**Fig. 1b**), were also increased in liver core biopsies from obese patients (BMI 36-61) with NAFL (NAS=1-2), when compared to those from obese patients (BMI 36-61) without steatosis (NAS=0) (32). Moreover, except for *NOX4* that trended lower, *NFE2L2*, *NQO1*, *SOD2*, *CAT* gene expression declined in obese patients (BMI 47-74) with NASH and fibrosis (NAS=5-6; fibrosis scores=1-2) to levels evident in obese patients with non-steatotic livers (**Fig. 1b**). Therefore, NAFL, but not obesity *per se* is accompanied by the increased expression of NFE2L2 targets genes, including *NOX4* that encodes a ROS producing enzyme, and *NQO1*, *SOD2* and *CAT* that encode key antioxidant defense enzymes, but these decline with more advanced disease and fibrosis.

As NOX4 and NFE2L2 are expressed in both hepatocytes and non-parenchymal cells, we next explored whether their induction in NAFL may be hepatocyte intrinsic. We assessed the expression of redox genes in the livers and hepatocytes of chow-fed lean versus high fat diet (HFD)-fed obese mice that develop liver steatosis, but do not progress to NASH/fibrosis. Hepatocytes from HFD-fed mice were steatotic, as reflected by the accumulation of lipids and the expression of lipogenic genes (**Fig. S1a-b**). As in humans, *Nfe2l2* and *Nox4* mRNA levels were induced in the livers (**Fig. 1c**) or hepatocytes (**Fig. 1d**) from HFD-fed mice. The induction of *Nfe2l2* in hepatocytes from HFD-fed mice was accompanied by the increased expression of NFE2L2 target genes (**Fig. 1e**) encoding enzymes involved in i) NADPH production necessary for the reduction of GSSG to GSH, including phosphoglycerate dehydrogenase (*Phgdh*), malic enzyme 1 (*Me1*), and glucose-6-phosphate dehydrogenase (*G6pd*), ii) GSH production and regeneration, including glutamate-cysteine ligase (GCL) catalytic subunit (*Gclc*), GCL complex modifier subunit (*Gclm*) and glutathione reductase (*Gsr*), iii) quinone detoxification, including NQO1 (*Nqo1*) and iv) ROS detoxification, including SOD-1 (*Sod1)* and -2 (*Sod2*), peroxiredoxin-3 (*Prdx3*) and catalase (*Cat*). Several of these genes were also increased in livers of HFD-fed mice (**Fig. S1c**). The expression of *Cybb* that encodes the $O2^{\bullet-}$producing enzyme NOX2, was modestly increased, whereas *Ncf1* and *Rac1* that encode the NOX2 regulatory subunits $p47^{phox}$ and RAC1 were not altered (**Fig. S1d**). The induction of *Nfe2l2* and *Nox4* in hepatocytes from HFD-fed mice was accompanied by increased NFE2L2 and NOX4 protein levels, as well as increased NQO1, SOD-2 and catalase (**Fig. 1f-h**) with no overt differences in NOX2, $p47^{phox}$ and RAC1 protein levels (**Fig. S1e**). Moreover, in line with the increased NFE2L2 and NFE2L2 transcriptional targets, the abundance of KEAP-1, which normally binds and targets NFE2L2 for degradation (33) was decreased (**Fig. 1f**). Finally, in line with the induction of NOX4 being an outcome of increased NFE2L2-dependent transcription, we found that the NFE2L2 agonist isothiocyanate sulforaphane readily induced *Nox4* in hepatocytes

(**Fig. S1f**). Thus steatosis in obesity is accompanied by the induction of NOX4 and the NFE2L2 antioxidant defense response in hepatocytes.

Lipids and mitochondrial ROS drive antioxidant defense in NAFLD

Chronic hepatic lipid accumulation in NAFLD is accompanied by increased mitochondrial $O2^{\bullet -}$ and H_2O_2 generation (9, 43). Accordingly, we determined the extent to which hepatic lipid accumulation and heightened mitochondrial ROS might influence antioxidant defense. We first compared ROS generation by hepatocytes isolated from chow-fed versus HFD-fed mice, to hepatocytes from chow-fed mice administered the saturated free fatty acid palmitate. We monitored for the emission of H_2O_2 from live hepatocytes using the H_2O_2-selective probe Amplex Red (Amplex® Red added to the culture medium). Hepatocytes from HFD-fed mice generated more ROS than hepatocytes from chow-fed mice (**Fig. 2a**). Also, hepatocytes from chow-fed mice treated with palmitate overnight generated more ROS than vehicle-treated controls (**Fig. 2b**; **Fig. S2a**). Importantly, the extent of palmitate-induced ROS generation approximated that seen in hepatocytes from HFD-fed mice (**Fig. 2b**); after more prolonged treatment, lipogenic gene expression was also increased (**Fig. S2b**) as noted in hepatocytes from HFD-fed mice. Next, we assessed if palmitate-induced ROS might be sufficient to drive the antioxidant defense response. Palmitate treatment significantly increased the expression of *Nfe2l2* (**Fig. 2c**) and NFE2L2 transcriptional targets, including *Nqo1*, *Sod1*, *Sod2*, *Cat* and *Nox4* (**Fig. 2d-e; Fig. S2c**); by contrast mRNAs for NOX2 subunits were unaltered (**Fig. 2e**). The palmitate-induced increase in *Nfe2l2* was accompanied by increased NFE2L2 and decreased KEAP-1 protein levels (**Fig. 2f**). Consistent with this, NOX4, NQO1, SOD2 and catalase protein levels were all increased (**Fig. 2f**). Indeed, NFE2L2, KEAP-1, NQO1, SOD1, catalase and NOX4 levels in palmitate-treated hepatocytes from chow-fed mice approximated those seen in hepatocytes isolated from HFD-fed mice (**Fig. 2f**). Finally, we

assessed if the palmitate-induced antioxidant defense response and *Nox4* expression might be ascribed to increased mitochondrial ROS generation. To this end, we assessed if the mitochondrial-targeted O2•⁻ scavenger and antioxidant mitoTEMPOL could reduce ROS and thereby antioxidant defense and *Nox4* expression. Treatment with mitoTEMPOL not only attenuated the palmitate-induced increase in H_2O_2 (**Fig. 2g**), but also the expression of the antioxidant defense genes *Nfe2l2*, *Nqo1*, *Sod1*, *Sod2* and *Cat* as well as the expression of *Nox4* (**Fig. 2h**). Therefore, heightened antioxidant defense response and the induction of NOX4 in NAFLD might be linked to the enhanced ROS production by mitochondria.

NOX4 is essential for antioxidant defense in hepatocytes

Previously we have shown that NFE2L2 drives *Nox4* expression in muscle and in turn, NOX4-derived H_2O_2 enhances NFE2L2 antioxidant defense to attenuate muscle oxidative damage and insulin resistance (44). In this study we have reaffirmed that the activation of NFE2L2 with sulforaphane is sufficient to induce *Nox4* expression in hepatocytes (**Fig. S1f**). We reasoned that the induction of NOX4 in hepatocytes in NAFLD might function as part of feedback loop to exacerbate and/or sustain NFE2L2 antioxidant defense otherwise instigated by mitochondrial ROS. To test this we isolated hepatocytes from control ($Nox4^{fl/fl}$) (45) and hepatocyte-specific NOX4-deficient mice (*Alb*-Cre;$Nox4^{fl/fl}$) fed a HFD for 10-weeks to induce steatosis (**Fig. S3a**) and assessed H_2O_2 levels and the expression of NFE2L2 and its target genes. NOX4 was effectively deleted in hepatocytes (**Fig. 3a-b**). The deletion of *Nox4* attenuated the otherwise increased H_2O_2 emission by hepatocytes from HFD-fed mice (**Fig. 3c**), but this still exceeded that from chow-fed $Nox4^{fl/fl}$ mice (**Fig. 3c**), consistent with both mitochondria and the induced NOX4 contributing to ROS generation. The deletion of *Nox4* also attenuated the expression of both *Nfe2l2* (**Fig. 3d**) and NFE2L2 target genes, including *Nqo1*, *Sod1*, *Sod2* and *Cat* (**Fig. 3e**), as well as the corresponding NFE2L2, NQO1, SOD2 and

catalase proteins (**Fig. 3f-g**). The reduced NFE2L2 and NQO1 could be rescued by incubating cells in the presence of the proteasome inhibitor MG132 (**Fig. 3g**), consistent with NOX4-derived H_2O_2 otherwise preventing NFE2L2 degradation. Conversely, the deletion of *Gpx1* encoding glutathione peroxidase (GPX)-1, an enzyme that detoxifies H_2O_2 increased the emission of H_2O_2 by hepatocytes from HFD-fed mice (**Fig. 3g**) and increased the expression of *Nfe2l2*, *Nqo1*, *Sod2* and *Cat* (**Fig. 3h**). Therefore, changes in H_2O_2 levels in hepatocytes from HFD-fed mice can elicit corresponding changes in antioxidant defense gene expression. The reduced expression of antioxidant defense genes and decreased NFE2L2 and NQO1 proteins associated with NOX4-deficiency in hepatocytes from HFD-fed mice were also evident in the livers of 12-week HFD-fed *Alb*-Cre;*Nox4*$^{fl/fl}$ versus *Nox4*$^{fl/fl}$ mice (**Fig. 3j; Fig. S3b**). The reduced antioxidant gene expression in hepatocytes from *Alb*-Cre;*Nox4*$^{fl/fl}$ HFD-fed mice was accompanied by reduced NFE2L2 and increased KEAP-1 protein levels, consistent with NOX4-derived ROS being required for the degradation of KEAP-1 and the stabilisation of NFE2L2 (**Fig. 3k; Fig. S3c**). Importantly, as with ROS production, NFE2L2 levels in hepatocytes from HFD-fed *Alb*-Cre;*Nox4*$^{fl/fl}$ mice tended to exceed those in hepatocytes from chow-fed *Nox4*$^{fl/fl}$ mice (**Fig. 3k; Fig. S3c**), consistent with both mitochondrial- and NOX4-derived ROS contributing to the antioxidant defense response. In line with this, SOD-2, NQO1 and catalase were attenuated by NOX4 deficiency, but still exceed those in hepatocytes from chow-fed *Nox4*$^{fl/fl}$ mice (**Fig. 3k; Fig. S3c**). Importantly, the reduced antioxidant defense gene expression (**Fig. 4a**) and NFE2L2, SOD-2, NQO1 and catalase protein levels (**Fig. 4b; Fig. S3d**) in hepatocytes from HFD-fed *Alb*-Cre;*Nox4*$^{fl/fl}$ mice could be corrected by the administration of the NFE2L2 agonist sulforaphane, consistent NOX4 deficiency abrogating NFE2L2-dependent responses. Finally, we found that NOX4-deficiency in hepatocytes from chow-fed *Alb*-Cre;*Nox4*$^{fl/fl}$ mice largely attenuated the palmitate-induced increase in antioxidant defense, as reflected by the expression of *Nfe2l2* and its target genes *Nqo1*, *Sod2*

and *Cat* (**Fig. 4c**). Thus the induction of NOX4 in NAFLD, downstream of mitochondrial ROS, may be required for optimal NFE2L2 antioxidant defense responses.

To specifically assess if NOX4-derived ROS in NAFLD contributes to antioxidant defense, we first assessed the impact of deleting *Gpx1*. The compound deletion of *Gpx1* corrected the diminished H_2O_2 levels (**Fig. 4d**) and the reduced antioxidant defense response (**Fig. 4e**) in hepatocytes from HFD-fed *Alb*-Cre;$Nox4^{fl/fl}$ mice. Next, to determine if the effects of NOX4 deletion were attributed to decreased NOX4 activity, we took advantage of the NOX1/4 inhibitor GKT137831 (46). We treated hepatocytes from HFD-fed $Nox4^{fl/fl}$ versus *Alb*-Cre;$Nox4^{fl/fl}$ mice with vehicle or GKT137831 and measured ROS production and antioxidant defense. GKT137831 was just as efficient as NOX4 deletion in reducing H_2O_2 levels (**Fig. 4f**). Since we could not detect *Nox1* in isolated hepatocytes by qPCR, we surmise that these effects are due to the inhibition of NOX4. Consistent with this, GKT137831 did not further reduce the emission of H_2O_2 by NOX4-deficient hepatocytes (**Fig. 4f**). The inhibition of NOX4 and the reduction in ROS production were accompanied by reductions in NFE2L2 targets genes (**Fig. 4g**) and corresponding proteins (**Fig. 4h**). Importantly, the decreased antioxidant defense associated with the inhibition of NOX4 could be corrected by the administration of the NFE2L2 agonist sulforaphane (**Fig. 4g-h**). Furthermore, GKT137831 repressed the palmitate-induced expression of *Nfe2l2* target genes, including *Nqo1*, *Sod2* and *Cat* (**Fig. 4i**). Taken together these results point towards the induction of NOX4 and the accompanying increased ROS in hepatocytes being essential for the antioxidant defense response that is instigated by mitochondrial ROS in NAFLD.

NOX4 deletion in hepatocytes promotes oxidative stress, insulin resistance and cell death

Numerous studies have shown that oxidative stress and in particular increased mitochondrial ROS can contribute to the development of insulin resistance (16, 17, 19, 47).

Indeed, the heterozygous deletion of *Sod2* and consequent increased mitochondrial $O2^{\bullet-}$ promotes insulin resistance in chow-fed mice, whereas SOD-2 overexpression, or the expression of mitochondrial-targeted catalase attenuate systemic insulin resistance in HFD-fed mice (16, 17, 19). Therefore, we reasoned that ablating NOX4 and abrogating the resultant H_2O_2-dependent NFE2L2 antioxidant defense response, and in particular reducing SOD-2, would promote mitochondrial oxidative stress to diminish insulin signalling and promote insulin resistance. To test this, we monitored by confocal microscopy for mitochondrial $O2^{\bullet-}$ levels using the mitochondrial $O2^{\bullet-}$ probe MitoSOX Red. The deletion of *Nox4* in hepatocytes increased mitochondrial $O2^{\bullet-}$ in NOX4-deficient hepatocytes isolated from HFD-fed mice (**Fig. 4a**). The increased mitochondrial $O2^{\bullet-}$ was accompanied by a reduction in insulin signalling, as monitored by AKT Ser-473 phosphorylation (p-AKT) in hepatocytes (**Fig. 5b; Fig. S4a**). Importantly, treatment with the NFE2L2 agonist sulforaphane not only restored the decreased antioxidant defense gene expression and the decreased abundance of the NFE2L2, NQO1, SOD-2 and catalase proteins (**Fig. 3k-l**), but also partially restored insulin signalling in NOX4-deficient hepatocytes (**Fig. 5c; Fig. S4b**). Moreover, treatment with the mitochondrial-targeted $O2^{\bullet-}$ scavenger mitoTEMPOL restored insulin signalling in hepatocytes from HFD-fed *Alb*-Cre;$Nox4^{fl/fl}$ mice (**Fig. 5d; Fig. S4c**). Finally, the sustained inhibition of NOX4 with GKT137831 diminished the expression of antioxidant defense genes (**Fig. 6a**) and insulin-induced p-AKT in hepatocytes from HFD-fed mice (**Fig. 6b**) and both were prevented if hepatocytes were additionally co-cultured with either sulforaphane (**Fig. 6c, d**), or the GSH precursor N-acetyl cysteine (NAC) (**Fig. 6e, f**). By contrast, the short-term administration of GKT137831 had no impact on insulin-induced p-AKT, arguing against NOX4-derived ROS having direct effects on insulin signalling (**Fig. S4d**). Therefore, defective NOX4-dependent antioxidant defense may exacerbate mitochondrial oxidative stress and the attenuation of insulin signalling in hepatocytes.

A potential outcome of defective antioxidant defense in NOX4-deficient hepatocytes in NAFLD might be increased oxidative damage. Consistent with this, we noted increased oxidative lipid damage, as assessed by immunoblotting NOX4-deficient hepatocytes from HFD-fed mice for 4-hydroxynonenal (4-HNE) (**Fig. 5e; Fig. S4e**), a marker of lipid peroxidation, as well as increased oxidative protein damage, as assessed by immunoblotting for protein carbonylation (**Fig. 5f; Fig. S4f**). The increased lipid peroxidation and protein carbonylation exceeded that otherwise induced in HFD-fed mice (**Fig. 5e-f**). The increased oxidative protein damage was attenuated when NOX4-deficient *Alb*-Cre;*Nox4*$^{fl/fl}$ hepatocytes were cultured with sulforaphane (**Fig. 5g**) that could rescue the defective antioxidant defense (**Fig. 4a-b**). Moreover, the increased oxidative protein damage was attenuated when NOX4-deficient *Alb*-Cre;*Nox4*$^{fl/fl}$ hepatocytes were cultured in the presence of mitoTEMPOL (**Fig. 5h**). Finally, the sustained inhibition of NOX4 with GKT137831 also increased oxidative protein damage in hepatocytes from HFD-fed mice (**Fig. 6g**) and this could be corrected when cells were co-cultured with sulforaphane (**Fig. 6h**) or NAC (**Fig. 6i**). These findings are consistent with the increased oxidative damage accompanying NOX4 deficiency being attributable to defective antioxidant defense and increased mitochondrial oxidative stress.

To test further if the increased oxidative damage may be attributed to enhanced oxidant sensitivity, we treated hepatocytes from HFD-fed *Nox4*$^{fl/fl}$ versus *Alb*-Cre;*Nox4*$^{fl/fl}$ mice with menadione. Menadione is a drug that generates ROS within the cytosol and mitochondria through futile redox cycling (48). Menadione increased the generation of ROS/H_2O_2 in hepatocytes isolated from HFD-fed mice (**Fig. 7a**); overall H_2O_2 generation was reduced by NOX4-deficiency, but the relative increase in menadione-induced H_2O_2 was similar (**Fig. 7a**). As expected, menadione treatment increased oxidative protein damage in both *Nox4*$^{fl/fl}$ and *Alb*-Cre;*Nox4*$^{fl/fl}$ hepatocytes **(Fig. S4g)**. However, the extent of oxidative damage was exacerbated by NOX4 deficiency **(Fig. S4g)**. A potential consequence of increased oxidative damage is cell

death, which in the context of the liver would elicit regenerative responses and lead to fibrosis. Consistent with this, menadione, which promotes cell death in a ROS-dependent manner (48), induced cell death (assessed by monitoring for metabolically active live cells) and this was exacerbated by NOX4-deficiency (IC50 *Nox4*$^{fl/fl}$=8.4 μM; IC50 *Alb*-Cre;*Nox4*$^{fl/fl}$=1.3 μM; **Fig. 7b**). Importantly, the enhanced menadione-induced cell death was blocked by sulforaphane or mitoTEMPOL (**Fig. 7c**), consistent with NOX4-deficiency exacerbating cell death because of defective NFE2L2 antioxidant defense and increased mitochondrial ROS. Moreover, the enhanced menadione-induced cell death in NOX4-deficient hepatocytes was accompanied by increased cleaved caspase-3 and cleaved PARP (poly ADP ribose polymerase), consistent with the promotion of apoptosis (**Fig. 7d**). The enhanced cell death was also accompanied by the increased phosphorylation and activation of the mitogen-activated protein kinases JNK and p38 (**Fig. 7d; S4h**), which are known to contribute to apoptosis and inflammatory responses in the liver (49, 50). Finally, the enhanced cleavage of caspase-3 and PARP and the increased p38 activation were reduced by treating hepatocytes with either mitoTEMPOL (**Fig. 7e**), or the NFE2L2 agonist sulforaphane (**Fig. S4i**). These results point towards the induction of NOX4 in the liver in obesity driving the antioxidant defense response to mitigate mitochondrial oxidative stress, macromolecular damage and cell death in lipid-laden hepatocytes.

Hepatocyte NOX4-deficiency promotes obesity, steatosis and insulin resistance in mice

To explore the impact of NOX4 abundance on hepatic pathophysiology in diet-induced obesity (DIO) we sought to delete *Nox4* postnatally in hepatocytes using the *Alb*-Cre transgene; *Nox4* was efficiently deleted in the livers and hepatocytes of *Alb*-Cre;*Nox4*$^{fl/fl}$ mice (**Fig. 3a-b**; **Fig. S5a-b**), but not in other metabolic tissues (**Fig. S5a-b**). 8-week-old *Nox4*$^{fl/fl}$ and *Alb*-Cre;*Nox4*$^{fl/fl}$ mice were fed either a standard chow-diet or a HFD for 12-weeks and effects on body weight, body composition, glucose metabolism and liver steatosis assessed. The deletion

of *Nox4* in hepatocytes had no effect on body weight in mice fed a chow-diet (**Fig. S5c**). By contrast, the deletion of hepatocyte *Nox4* in HFD-fed male (**Fig. 8a**) or female mice (**Fig. S6a**) increased body weight. The increased body weight in male mice was accompanied by increased food intake in the dark cycle, but paradoxically also increased energy expenditure, as determined by indirect calorimetry (**Fig. S7a-c; Fig. S8**). NOX4-deficiency increased whole-body adiposity and fat pad weights in HFD-fed but not chow-fed mice, without any change in lean mass (**Fig. 8b-c; Fig. S5d-e; Fig. S6b**). Liver weights were also increased in HFD-fed (**Fig. 8c; Fig. S6c)** but not chow-fed *Alb*-Cre;*Nox4*$^{fl/fl}$ mice (**Fig. S5e**) and this was accompanied by increased steatosis, as assessed histologically monitoring for lipid droplets (H&E) and staining for neutral lipids with Oil Red O (**Fig. 8d; Fig. S6d)**; steatosis was not evident in chow-fed *Alb*-Cre;*Nox4*$^{fl/fl}$ mice (**Fig. S5f**). The increased steatosis was in turn accompanied by the increased expression of *de novo* lipogenesis genes, including *Fasn*, *Scd1* and *Srebf1* (**Fig. 8e),** increased hepatic FASN and SCD1 protein levels (**Fig. 8f)** and an ~2-fold increase in *de novo* lipogenesis (**Fig. 8g)**, as assessed in liver slices *ex vivo*, without any significant change in fatty acid oxidation (**Fig. 6h)**. The enhanced *de novo* lipogenesis is consistent with studies that have shown that NFE2L2 negatively regulates lipid synthesis genes in the liver and protects from steatosis (35, 36, 51-53). Indeed, we found that the expression of the lipogenesis genes *Fasn* and *Scd1* were also induced in GKT137831-treated hepatocytes (**Fig. S9a**) from HFD-fed mice where antioxidant defense was defective (**Fig. 6a**). However, the enhanced lipogenic gene expression in NOX4-deficient hepatocytes from HFD-fed mice was corrected by administering the NFE2L2 agonist sulforaphane (**Fig. S9b)**. Irrespective, consistent with the overt steatosis, triglyceride, diglyceride and ceramide levels were significantly elevated in HFD-fed *Alb*-Cre;*Nox4*$^{fl/fl}$ mice (**Fig. 8i)**. Therefore, the deletion of NOX4 in hepatocytes exacerbates DIO and promotes steatosis attributable, at least in part, to increased *de novo* lipogenesis.

An expected outcome of DIO in C57BL/6 mice is the development of insulin resistance. Consistent with this, HFD-fed *Alb*-Cre;*Nox4*$^{fl/fl}$ mice were more insulin resistant, as reflected in insulin tolerance tests (**Fig. 9a; Fig. S6e-f)** and the heightened circulating glucose and insulin in fasted mice (**Fig. 9b; Fig. S6f)**. To explore the impact of NOX4-deficiency on glucose turnover and whole-body insulin sensitivity, we subjected 12-week HFD-fed conscious and free-moving *Nox4*$^{fl/fl}$ versus *Alb*-Cre;*Nox4*$^{fl/fl}$ male mice to hyperinsulinemic-euglycemic clamps. We found that the glucose infusion rate (GIR) necessary to maintain euglycemia during the insulin-clamp was reduced (**Fig. 9c; Fig. S7d-e**), consistent with the development of insulin resistance. The rate of glucose disappearance (RD), a measure of muscle and adipose tissue glucose uptake, was reduced in clamped *Alb*-Cre;*Nox4*$^{fl/fl}$ mice (**Fig. 9d)**, whereas endogenous glucose production (EGP) in clamped *Alb*-Cre;*Nox4*$^{fl/fl}$ mice was increased (**Fig. 9e; Fig. S7f-g)**, consistent with hepatic insulin resistance. The latter was accompanied by the increased expression of genes encoding glucose-6 phosphatase (*G6pc*) and phosphoenolpyruvate carboxykinase (*Pck1*) (**Fig. 9f)**, rate-limiting enzymes in gluconeogenesis. The diminished insulin-induced repression of HGP in HFD-fed *Alb*-Cre;*Nox4*$^{fl/fl}$ mice was also associated with a reduction in insulin-induced PI3K/AKT signalling, as assessed by immunoblotting for AKT Ser-473 phosphorylation in corresponding liver homogenates (**Fig. 9g),** or in hepatocytes from HFD-fed *Alb*-Cre;*Nox4*$^{fl/fl}$ mice (**Fig. 5b-d**). Taken together, our results are consistent with NOX4 deficiency in the liver diminishing antioxidant defense to promote hepatic and systemic insulin resistance in obesity.

Hepatocyte NOX4-deficiency promotes NASH and fibrosis

C57BL/6 mice fed a HFD become obese and develop NAFL, but do not develop NASH (54). Beyond exacerbating steatosis and insulin resistance, hepatocyte NOX4-deficiency in HFD-fed C57BL/6 mice also facilitated the progression to NASH (**Fig. 7**), with many of the

key diagnostic features of human NASH (1), including hepatocyte ballooning (**Fig. 10a-b**), hepatocyte cell death, as reflected by TUNEL staining (**Fig. 10c**), and lymphocytic infiltrates, including $CD3^+$ T cell infiltrates, as assessed by histology (**Fig. 10d**), immunohistochemistry (**Fig. 10e**) or flow cytometry (**Fig. 10f; Fig. S10**). The lymphocytic infiltrates included $CD4^+$ and $CD8^+$ T cells with an effector/memory phenotype ($CD44^{hi}CD62L^{lo}$), including antigen-experienced ($CD49d^{hi}$) and activated ($CD69^{hi}$) $CD8^+$ T cells, as well as those with terminally-differentiated ($KLRG1^{hi}$) and exhausted ($PD\text{-}1^{hi}TIM\text{-}3^{hi}$) phenotypes (**Fig. 10f; Fig. S10**), as seen previously in humans with NASH (32, 54-56). It also included 'autoaggressive' $PD\text{-}1^{hi}CXCR6^{hi}$ $CD8^+$ T cells (**Fig. 10f**) that have been proposed to contribute to NAFLD pathogenesis in humans (57). Natural killer (NK) cells, dendritic cells (DCs), natural killer T cells (NKT), macrophages and Kupffer cells that are frequently elevated in NASH (56) were also increased (**Fig. 10f; Fig. S10**), as were immunosuppressive $CD4^+$ regulatory T cells (**Fig. 10f**). The increased T cell infiltration was in turn accompanied by increased inflammation, as reflected by heightened STAT-1 Y701 phosphorylation (p-STAT-1) in hepatocytes (**Fig. 11a**), the expression of the STAT-1 target gene *Cxcl9* (encodes T cell chemoattractant CXCL9) and the increased expression of genes encoding proinflammatory cytokines, including IFNγ (*Ifng*) and TNF (*Tnf*) (**Fig. 11b**). An expected consequence of T cell recruitment and activation, inflammation and hepatocyte cell death in NAFLD is the induction of reparative processes that lead to DNA damage in dividing hepatocytes and increased fibrosis due to hepatic stellate cell activation. Consistent with this, hepatocytes with dsDNA breaks (γH2AX staining) were readily evident in the livers in HFD-fed *Alb*-Cre;$Nox4^{fl/fl}$ mice (**Fig. 11c**). In addition, livers in HFD-fed *Alb*-Cre;$Nox4^{fl/fl}$ mice exhibited overt signs of fibrosis, as reflected by Picrosirius red staining (stains collagen) (**Fig. 11d**), the increased expression of fibrosis-related genes, including *Acta2* (α-smooth muscle actin) and *Tgfb* (transforming growth factor β), indicative of stellate cell activation, and the extracellular matrix genes *Col1a1* (α-1 type-1 collagen) and

Fn1 (fibronectin) (**Fig. 11e**), as well as the increased abundance of hydroxyproline (**Fig. 11f**), a measure collagen degradation and the severity of fibrosis. Thus the deletion of NOX4 in the liver not only promotes steatosis, but also facilitates the transition to NASH and ensuing fibrosis in DIO.

Next, we determined whether the deletion of NOX4 might be sufficient to drive NASH/fibrosis in adult mice that are already obese with established steatosis. To this end we sought to delete *Nox4* using an adeno-associated viral (AAV)-thyroxine binding globulin (TBG) promoter construct that expresses Cre specifically in hepatocytes (58). 8-week-old $Nox4^{fl/fl}$ mice were HFD-fed for 10-weeks to promote obesity and steatosis and then administered either AAV-TBG-EGFP control, or AAV-TBG-iCre and high fat feeding continued for a further 10-weeks. The administration of AAV-TBG-iCre efficiently deleted *Nox4* so that *Nox4* mRNA was reduced by approximately 70% and NOX4 protein by 60% (**Fig. 12a-b**). The deletion of *Nox4* was accompanied by modest increases in body weight (**Fig. 12c**) attributed to increased whole-body adiposity (**Fig. 12d**). The deletion of *Nox4* was also accompanied by the decreased hepatic expression of antioxidant defense genes, including *Nfe2l2*, *Nqo1*, *Sod1*, *Sod2*, *Prdx1* and *Catalase* (**Fig. 12e**) and reduced NFE2L2 (**Fig. 12f**), increased KEAP-1 (**Fig. 12f**) and decreased NQO1, SOD-2 and catalase proteins (**Fig. 12f**), consistent with an abrogated antioxidant defense response. Moreover, *Nox4* deletion increased steatosis (**Fig. 12g**) and the expression of lipogenic genes (**Fig. 12h**). Notably, the deletion of hepatocyte *Nox4* in adult obese mice also facilitated the transition to NASH with fibrosis, as assessed histologically by Picrosirius red staining (**Fig. 12i**), by measuring the hepatic expression of inflammatory (*Tnf*, *Ifng*) and fibrosis-related (*Acta2*, *Tgfb*, *Col1a1*, *Fn1*) genes (**Fig. 12j**), and by measuring hepatic hydroxyproline levels (**Fig. 12k**). Therefore, the deletion of hepatocyte *Nox4* in adult obese mice can abrogate the antioxidant defense response

otherwise induced during NAFL to exacerbate steatosis and facilitate the transition to NASH/fibrosis.

To explore if the progression to NASH/fibrosis associated with the deletion of *Nox4* might be ascribed to decreased NOX4-derived ROS generation and antioxidant defense, we determined if the NOX1/4 inhibitor GKT137831 could promote NASH/fibrosis in HFD-fed C57BL/6 mice (**Fig. 13**). The administration of GKT137831 (40 mg/kg, 3x/week, 5-weeks) to 15-week HFD-fed obese C57BL/6 mice modestly increased body weights (**Fig. 13a**) and had no significant effect on liver weights (**Fig. 13b**), but decreased *Nfe2l2* expression in the liver along with the expression of key antioxidant defense genes, including *Sod1*, *Sod2*, *Catalase* and *Nqo1* (**Fig. 13c**), while increasing the expression of lipogenic genes (**Fig. 13d; Fig. S9a**). This was accompanied by increased steatosis (**Fig. 13e**) and lymphocytic infiltrates (**Fig. 13f**), as well as increased fibrosis (**Fig. 13g-h**), as assessed by the hepatic expression of fibrosis-related genes (**Fig. 13g**) and by histology (**Fig. 13h**). These results are consistent with the induction of NOX4 in the livers of obese mice with steatosis driving ROS-dependent antioxidant defense to limit steatosis, mitochondrial oxidative stress and tissue damage and attenuate the progression to NASH/fibrosis.

Reduced NOX4 and antioxidant defense gene expression in NASH with advanced fibrosis

Our analysis of publicly available RNAseq data (41) and our qPCR analyses of liver core biopsies revealed that *NOX4* and antioxidant genes tended to decline in humans with NASH and advanced fibrosis when compared to those with NAFL (**Fig. 1a**). We reasoned that the decline in *NOX4* and antioxidant defense may exacerbate disease and contribute to NASH/fibrosis. Accordingly, we first asked if the reduced *NOX4* and antioxidant defense gene expression might have been hepatocyte intrinsic, or otherwise, indicative of changes in the abundance/activation of non-parenchymal cells in NASH/fibrosis. To this end we isolated

hepatocytes from C57BL/6 mice that were fed either a standard chow-diet, a HFD to promote obesity, insulin resistance and steatosis, or a choline-deficient HFD (CD-HFD) to promote obesity, insulin resistance and the progression to NASH/fibrosis. CD-HFD-fed mice exhibited NASH with steatosis, lymphocytic infiltrates and fibrosis (**Fig. 14a-b**). As noted already, *Nox4*, *Sod2*, *Cat* and *Nqo1* mRNA levels were increased in lipid-laden hepatocytes from HFD-fed C57BL/6 (**Fig. 14c; Fig. S11**). Importantly, as noted in humans with NASH and advanced fibrosis, *Nox4*, *Sod2*, *Cat* and *Nqo1* were reduced in hepatocytes from CD-HFD fed mice (**Fig. 14c**). The reduced expression of *Nox4*, *Sod2*, *Cat* and *Nqo1* was accompanied by decreased NOX4, NQO1, SOD2 and catalase protein levels (**Fig. 14d**) and reduced H_2O_2 production (**Fig. 14e**). Importantly, the reduced NOX4 and H_2O_2 and the decreased expression of antioxidant defense proteins in hepatocytes from CD-HFD fed mice, was in turn accompanied by increased oxidative protein damage (**Fig. 14f**). To independently assess the extent to which NASH and fibrosis may impact on *Nox4* expression *in vivo* we took advantage of a publicly-available cell type-resolved transcriptional dataset (59) to assess the expression of *Nox4*, as well as the expression of antioxidant defense genes in hepatocyte nuclei from mice fed a low-fat control diet versus a HFD rich in fructose, palmitate and cholesterol (HFD/FPC diet) for 20-weeks; the HFD/FPC diet promotes variable degrees of NASH and fibrosis and recapitulates key aspects of human NASH (59). We found that *Nox4*, *Sod1*, *Sod2*, *Cat*, *Nfe2l2* and *Nqo1* mRNA levels were increased in hepatocytes from HFD/FPC mice with mild NASH with minimal inflammation and no appreciable fibrosis (**Fig. 14g**), but tended to decline in hepatocytes in mice with advanced NASH with comparable levels of steatosis but more inflammatory foci and overt fibrosis (**Fig. 14g**). Therefore, the decline in NOX4 and NFE2L2 antioxidant defense associated with more advanced NASH/fibrosis may contribute to disease progression. To test this, we sought to overexpress NOX4 and ascertain whether this might sustain the antioxidant defense response and temper NASH/fibrosis in mice fed a CD-HFD. We took advantage of

AAVs to overexpress either GFP (AAV-TBG-EGFP) or murine NOX4 (AAV-TBG-m*Nox4*) in hepatocytes before feeding mice a CD-HFD for 12-weeks. Hepatic *Nox4* was overexpressed by 7.9-fold (**Fig. 15a**) and this was accompanied by increased NOX4 protein (**Fig. 15b**) and a >2-fold increase in extracellular H_2O_2 in isolated hepatocytes (**Fig. 15c**). The overexpression of NOX4 was accompanied by modestly decreased body (**Fig. 15d**) and liver weights (**Fig. 15e**) but no change in body composition (**Fig. 15f**). The decreased liver weight was accompanied by the decreased expression of lipogenic genes (**Fig. 15g**) and decreased steatosis (**Fig. 15h**). Moreover, the overexpression of NOX4 increased the hepatic expression of select antioxidant defense genes (**Fig. 15i**) and proteins, including NFE2L2, SOD2 and NQO1 (**Fig. 15j; Fig. S12**) and decreased oxidative damage as assessed by monitoring for protein carbonylation in hepatocytes from the corresponding mice (**Fig. 15k**). The decreased oxidative damage was accompanied by a trend for decreased hepatic $CD8^+$ T cell infiltrates including decreased activated and effector/memory $CD8^+$ T cells and a significant decrease in the proportion of exhausted and 'autoaggressive' $CD8^+$ T cells (**Fig. 16a**); innate immune cells remained unaltered (**Fig. 16a**). In addition, CD-HFD-fed mice overexpressing NOX4 were characterised by a trend for decreased hepatic inflammation, as assessed by the decreased immune infiltrates (**Fig. 16b**) and the decreased expression of proinflammatory genes (**Fig. 16c**). This was accompanied by decreased fibrosis, as assessed histologically (**Fig. 16d**), the expression of fibrosis-related genes (**Fig. 16e**) and hepatic hydroxyproline levels (**Fig. 16f**). Therefore, forced NOX4 overexpression can mitigate NASH/fibrosis otherwise associated with the decline in *Nox4* in mice fed a NASH/fibrosis-promoting CD-HFD.

DISCUSSION

In this study we report that the induction of the NFE2L2 antioxidant defense response in NAFL, orchestrated by mitochondrial- and thereon NOX4-derived ROS, prevents liver damage and the progression to NASH with fibrosis. Conversely, reduced NOX4 and antioxidant defense might be a key feature of the progression to NASH and fibrosis.

The dysregulation of redox balance resulting in oxidative stress can affect the progression of many human diseases (60). In particular, the increased production of mitochondrial oxidants in metabolic tissues has been causally linked to the development of insulin resistance (10, 15-21, 23, 28, 61, 62), a key pathological feature of type 2 diabetes and a leading risk factor of NAFLD (1). Genetic and pharmacological studies in rodents also point toward mitochondrial oxidative distress facilitating the progression to NASH/fibrosis (9, 10, 14, 20-22). However, beyond the potential to drive disease progression, ROS also have important physiological functions (60). For example, ROS such as H_2O_2 can function as second messengers to facilitate signalling in response to physiological stimuli by oxidising and inactivating protein tyrosine phosphatases (63). Moreover, we have shown previously that H_2O_2 generated by NOX4 in skeletal muscle in mice during exercise can activate NFE2L2 and elicit adaptive responses that enhance muscle function and maintain insulin sensitivity (44). Similarly, others have reported that NOX4 also activates NFE2L2 in the heart to prevent oxidative stress and maintain cardiac function during exercise (64), whereas studies in humans have shown that antioxidants can negate the beneficial effects of exercise on insulin sensitivity and this is accompanied by the decreased expression of muscle genes encoding mediators of antioxidant defense, including SOD-1/2 and GPX-1 (65). Therefore, beyond directly affecting signalling and physiological processes, ROS also drive adaptive responses that mitigate disease.

In this study we have shown that mitochondrial- and NOX4-derived ROS function in concert to elicit adaptive responses in the liver to temper NAFLD pathogenesis. We have shown that mitochondrial- and NOX4-derived ROS drive NFE2L2 antioxidant defense in hepatocytes to limit the oxidative damage of macromolecules, the development of insulin resistance and the progression to NASH/fibrosis. Our studies indicate that this response is graded, with mitochondrial ROS first stabilising NFE2L2 to thereon increase the expression of NOX4, to further increase ROS/H_2O_2 and the abundance of NFE2L2, to thereby drive a robust antioxidant defense response. The importance of mitochondria-derived ROS/H_2O_2 in driving such adaptive/protective responses in the liver has been noted previously. Carter *et al.* reported that the beneficial effects of static magnetic and electric fields on insulin sensitivity were reliant in mitochondrial-derived O2•⁻ (66). Our own studies have shown the deletion of *Gpx1* in hepatocytes and the resultant increased H_2O_2 levels enhance insulin sensitivity in HFD-fed mice and attenuate NASH/fibrosis in mice fed a choline-deficient amino acid-defined (CDAA) diet (67). In this study, we report that ROS generation by NOX4 is essential for the mitochondrial-orchestrated adaptive response in NAFLD. The deletion of *Nox4* increased KEAP-1 and decreased NFE2L2 protein levels, thereby reducing the expression of NFE2L2 target genes, including those encoding SOD-2 and catalase. Previous studies have shown that the heterozygous deletion of *Sod2* in mice can promote mitochondrial oxidative stress (16), whereas genetic polymorphisms in *SOD2* in humans that decrease SOD-2 mitochondrial targeting and activity may be associated with NASH and the severity of fibrosis (22, 68). Thus, we propose that the reductions in SOD-2 and catalase would be key contributors to the oxidative distress evident in NOX4-deficient hepatocytes. The promotion of mitochondrial oxidative stress associated with the deletion/inhibition of NOX4 in hepatocytes diminished insulin signalling, whereas NOX4 deficiency *in vivo* promoted hepatic and systemic insulin resistance, a key driver of NAFLD. The deletion of *Nox4* and the diminished antioxidant

defense also exacerbated the ability of mitochondrial oxidants to promote hepatocyte cell death. The progression to NASH/fibrosis in HFD-fed *Alb*-Cre;*Nox4*$^{fl/fl}$ mice was accompanied by hepatocyte cell death, inflammation and the recruitment/accumulation of $CD8^+$ T cell subsets that have been causally linked with NASH (32, 54-57). The extent to which the progression to NASH/fibrosis may have been ascribed to oxidant-dependent cell death and ensuing inflammation, or otherwise to the oxidative inactivation of tyrosine phosphatases and the promotion of STAT-1 signalling in hepatocytes to drive T cell recruitment, inflammation and cell death as we have noted previously (32) remains unclear. Since both DNA damage and heightened hepatocyte STAT-1 signalling were readily evident, we propose that both mechanisms are likely to contribute. Interestingly, the deletion of *Nox4* in hepatocytes also increased DIO and enhanced steatosis, which is a risk factor for the progression to NASH. Although the molecular basis for the increased body weight in HFD-fed *Alb*-Cre;*Nox4*$^{fl/fl}$ mice remains unclear, food consumption was increased pointing towards potential crosstalk with the CNS and the control of feeding. The increased body weight/adiposity and systemic insulin resistance in HFD-fed *Alb*-Cre;*Nox4*$^{fl/fl}$ mice may have contributed to the increased steatosis by promoting the flux of lipids from adipose tissue. However, the increased steatosis was also accompanied by increased *de novo* lipogenesis. Previous studies have shown that NFE2L2 can negatively regulate the expression of lipid synthesis genes and protect from steatosis (35, 36, 51-53). Consistent with this we found that the increased hepatocyte lipogenic gene expression resulting from the deletion of *Nox4* was corrected by the administration of the NFE2L2 agonist sulforaphane. However, neither obesity *per se* nor steatosis are sufficient to drive the progression from NAFL to NASH in C57BL/6 mice or indeed humans (1, 7, 8). Therefore, although the increased weight gain and steatosis may have influenced disease severity, they would not have instigated disease progression.

Our findings seemingly contrast with previous studies that have reported that the deletion of *Nox4* in hepatocytes attenuates NASH/fibrosis in mice fed diets that promote NASH/fibrosis, with or without obesity (24). Yet other studies have shown that systemic NOX1/NOX4 inhibition with GKT137831 can repress liver fibrosis induced by bile duct ligation or CCl_4 treatment (46, 69). Our studies do not preclude NOX4-derived ROS in the context of diminished antioxidant defense contributing to oxidative distress and NAFLD pathogenesis. Moreover, our findings do not preclude a role for NOX1/NOX4 in other cell types, including hepatic stellate cells, where NOX1/4 activation may drive an activated/fibrogenic state (70). Our studies demonstrate that whereas steatosis and resultant increases in mitochondrial ROS drive *NOX4* expression in NAFL, the progression towards more advanced disease with fibrosis is accompanied by reduced *NOX4* and concomitantly reduced antioxidant defense. This is consistent with other studies that have shown that catalase activity declines in patients with overt NASH/fibrosis (10), as well as studies showing that hepatic *Nox4* and *Cat* transcripts are reduced in mice fed a NASH/fibrosis-promoting MCD diet (71). Importantly, we found that NOX4 overexpression in hepatocytes was able to increase antioxidant defense and decrease steatosis, inflammation and fibrosis in mice fed a NASH/fibrosis-promoting CD-HFD. Precisely why NOX4 and the antioxidant defense response may decline in NASH/fibrosis remains unclear, but may relate to the mitochondrial dysfunction associated with advanced disease (9, 10, 72). Irrespective, in the context of reduced NOX4 and resultant decreased adaptive antioxidant defense, any ROS generated by NOX4 might thereon contribute to oxidative distress and exacerbate disease severity, so that its complete deletion or inhibition would be beneficial. This is line with NOX4 contributing to both adaptive redox signalling to mitigate NAFLD progression, as well oxidative distress to promote NASH pathogenesis.

The results of this study underscore the importance of redox balance in governing the transition from NAFL to NASH and the progressive development of fibrosis in obesity. Our studies define the interplay between mitochondria and NOX4 in eliciting optimal NFE2L2-dependent antioxidant defense in hepatocytes and point towards perturbations in this adaptive response being an important contributor to NAFLD pathogenesis.

MATERIALS AND METHODS

Experimental procedures and reagents can be found in ***Supplemental Data***.

Statistics

Statistical significance was set at $P < 0.05$ and determined with a 2-tailed Student's t test, or Mann-Whitney U Test, or a one-way or two-way ANOVA with multiple comparisons.

Study approval

Animal experiments were approved by the Monash University School of Biomedical Sciences Animal Ethics Committee (Project IDs: 22138;23077;36631;17687;14368).

Use of human tissue was approved by the Monash University Human Research Ethics Committee (CF12/2339-2012001246; CF15/3041-2015001282). Subjects gave written consent before participating in the study. Liver core biopsies were from obese men and women undergoing bariatric surgery (32) and were processed for RNA isolation. Gender difference analyses were not performed due to the low frequency of suitable donors.

Data Availability

All data are available from the corresponding author or provided in the Supporting data values file.

REFERENCES

1. Loomba R, Friedman SL, and Shulman GI. Mechanisms and disease consequences of nonalcoholic fatty liver disease. *Cell.* 2021;184(10):2537-64.
2. Younossi Z, Anstee QM, Marietti M, Hardy T, Henry L, Eslam M, et al. Global burden of NAFLD and NASH: trends, predictions, risk factors and prevention. *Nat Rev Gastroenterol Hepatol.* 2018;15(1):11-20.
3. Younossi ZM, Golabi P, de Avila L, Paik JM, Srishord M, Fukui N, et al. The global epidemiology of NAFLD and NASH in patients with type 2 diabetes: A systematic review and meta-analysis. *J Hepatol.* 2019;71(4):793-801.
4. Huang DQ, El-Serag HB, and Loomba R. Global epidemiology of NAFLD-related HCC: trends, predictions, risk factors and prevention. *Nat Rev Gastroenterol Hepatol.* 2021;18(4):223-38.
5. Estes C, Razavi H, Loomba R, Younossi Z, and Sanyal AJ. Modeling the epidemic of nonalcoholic fatty liver disease demonstrates an exponential increase in burden of disease. *Hepatology.* 2018;67(1):123-33.
6. Bence KK, and Birnbaum MJ. Metabolic drivers of non-alcoholic fatty liver disease. *Mol Metab.* 2021;50:101143.
7. Jornayvaz FR, Birkenfeld AL, Jurczak MJ, Kanda S, Guigni BA, Jiang DC, et al. Hepatic insulin resistance in mice with hepatic overexpression of diacylglycerol acyltransferase 2. *Proc Natl Acad Sci USA.* 2011;108(14):5748-52.
8. Wu JW, Wang SP, Alvarez F, Casavant S, Gauthier N, Abed L, et al. Deficiency of liver adipose triglyceride lipase in mice causes progressive hepatic steatosis. *Hepatology.* 2011;54(1):122-32.
9. Karkucinska-Wieckowska A, Simoes ICM, Kalinowski P, Lebiedzinska-Arciszewska M, Zieniewicz K, Milkiewicz P, et al. Mitochondria, oxidative stress and nonalcoholic fatty liver disease: A complex relationship. *Eur J Clin Invest.* 2022;52(3):e13622.
10. Koliaki C, Szendroedi J, Kaul K, Jelenik T, Nowotny P, Jankowiak F, et al. Adaptation of Hepatic Mitochondrial Function in Humans with Non-Alcoholic Fatty Liver Is Lost in Steatohepatitis. *Cell Metab.* 2015;21(5):739-46.
11. Sunny NE, Parks EJ, Browning JD, and Burgess SC. Excessive hepatic mitochondrial TCA cycle and gluconeogenesis in humans with nonalcoholic fatty liver disease. *Cell Metab.* 2011;14(6):804-10.
12. Kussmaul L, and Hirst J. The mechanism of superoxide production by NADH:ubiquinone oxidoreductase (complex I) from bovine heart mitochondria. *Proc Natl Acad Sci USA.* 2006;103(20):7607-12.
13. Paradies G, Petrosillo G, Pistolese M, and Ruggiero FM. Reactive oxygen species affect mitochondrial electron transport complex I activity through oxidative cardiolipin damage. *Gene.* 2002;286(1):135-41.
14. Eccleston HB, Andringa KK, Betancourt AM, King AL, Mantena SK, Swain TM, et al. Chronic exposure to a high-fat diet induces hepatic steatosis, impairs nitric oxide bioavailability, and modifies the mitochondrial proteome in mice. *Antioxid Redox Signal.* 2011;15(2):447-59.
15. Fazakerley DJ, Chaudhuri R, Yang P, Maghzal GJ, Thomas KC, Krycer JR, et al. Mitochondrial CoQ deficiency is a common driver of mitochondrial oxidants and insulin resistance. *eLife.* 2018;7:e32111.
16. Hoehn KL, Salmon AB, Hohnen-Behrens C, Turner N, Hoy AJ, Maghzal GJ, et al. Insulin resistance is a cellular antioxidant defense mechanism. *Proc Natl Acad Sci USA.* 2009;106(42):17787-92.

17. Lee HY, Lee JS, Alves T, Ladiges W, Rabinovitch PS, Jurczak MJ, et al. Mitochondrial-Targeted Catalase Protects Against High-Fat Diet-Induced Muscle Insulin Resistance by Decreasing Intramuscular Lipid Accumulation. *Diabetes.* 2017;66(8):2072-81.
18. Paglialunga S, Ludzki A, Root-McCaig J, and Holloway GP. In adipose tissue, increased mitochondrial emission of reactive oxygen species is important for short-term high-fat diet-induced insulin resistance in mice. *Diabetologia.* 2015;58(5):1071-80.
19. Anderson EJ, Lustig ME, Boyle KE, Woodlief TL, Kane DA, Lin CT, et al. Mitochondrial H2O2 emission and cellular redox state link excess fat intake to insulin resistance in both rodents and humans. *J Clin Invest.* 2009;119:573-81.
20. Perry RJ, Kim T, Zhang XM, Lee HY, Pesta D, Popov VB, et al. Reversal of hypertriglyceridemia, fatty liver disease, and insulin resistance by a liver-targeted mitochondrial uncoupler. *Cell Metab.* 2013;18(5):740-8.
21. Perry RJ, Zhang D, Zhang XM, Boyer JL, and Shulman GI. Controlled-release mitochondrial protonophore reverses diabetes and steatohepatitis in rats. *Science.* 2015;347(6227):1253-6.
22. Al-Serri A, Anstee QM, Valenti L, Nobili V, Leathart JB, Dongiovanni P, et al. The SOD2 C47T polymorphism influences NAFLD fibrosis severity: evidence from case-control and intra-familial allele association studies. *J Hepatol.* 2012;56(2):448-54.
23. Satapati S, Kucejova B, Duarte JA, Fletcher JA, Reynolds L, Sunny NE, et al. Mitochondrial metabolism mediates oxidative stress and inflammation in fatty liver. *J Clin Invest.* 2015;125(12):4447-62.
24. Bettaieb A, Jiang JX, Sasaki Y, Chao TI, Kiss Z, Chen X, et al. Hepatocyte Nicotinamide Adenine Dinucleotide Phosphate Reduced Oxidase 4 Regulates Stress Signaling, Fibrosis, and Insulin Sensitivity During Development of Steatohepatitis in Mice. *Gastroenterology.* 2015;149(2):468-80 e10.
25. Nakagawa H, Umemura A, Taniguchi K, Font-Burgada J, Dhar D, Ogata H, et al. ER stress cooperates with hypernutrition to trigger TNF-dependent spontaneous HCC development. *Cancer Cell.* 2014;26(3):331-43.
26. Ding LG, Sun WF, Balaz M, He AY, Klug M, Wieland S, et al. Peroxisomal beta-oxidation acts as a sensor for intracellular fatty acids and regulates lipolysis. *Nat Metab.* 2021;3(12):1648-1661.
27. Martyn KD, Frederick LM, von Loehneysen K, Dinauer MC, and Knaus UG. Functional analysis of Nox4 reveals unique characteristics compared to other NADPH oxidases. *Cell Signal.* 2006;18(1):69-82.
28. Gurzov EN, Tran M, Fernandez-Rojo MA, Merry TL, Zhang X, Xu Y, et al. Hepatic oxidative stress promotes insulin-STAT-5 signaling and obesity by inactivating protein tyrosine phosphatase N2. *Cell Metab.* 2014;20(Jul 1):85-102.
29. He G, Yu GY, Temkin V, Ogata H, Kuntzen C, Sakurai T, et al. Hepatocyte IKKbeta/NF-kappaB inhibits tumor promotion and progression by preventing oxidative stress-driven STAT3 activation. *Cancer Cell.* 2010;17(3):286-97.
30. Seki S, Kitada T, Yamada T, Sakaguchi H, Nakatani K, and Wakasa K. In situ detection of lipid peroxidation and oxidative DNA damage in non-alcoholic fatty liver diseases. *J Hepatol.* 2002;37(1):56-62.
31. Videla LA, Rodrigo R, Orellana M, Fernandez V, Tapia G, Quinones L, et al. Oxidative stress-related parameters in the liver of non-alcoholic fatty liver disease patients. *Clin Sci (Lond).* 2004;106(3):261-8.
32. Grohmann M, Wiede F, Dodd GT, Gurzov EN, Ooi GJ, Butt T, et al. Obesity Drives STAT-1-Dependent NASH and STAT-3-Dependent HCC. *Cell.* 2018;175(5):1289-306.

33. Baird L, and Yamamoto M. The Molecular Mechanisms Regulating the KEAP1-NRF2 Pathway. *Mol Cell Biol.* 2020;40(13).
34. Kwak MK, Itoh K, Yamamoto M, and Kensler TW. Enhanced expression of the transcription factor Nrf2 by cancer chemopreventive agents: role of antioxidant response element-like sequences in the nrf2 promoter. *Mol Cell Biol.* 2002;22(9):2883-92.
35. Chowdhry S, Nazmy MH, Meakin PJ, Dinkova-Kostova AT, Walsh SV, Tsujita T, et al. Loss of Nrf2 markedly exacerbates nonalcoholic steatohepatitis. *Free Radic Biol Med.* 2010;48(2):357-71.
36. Meakin PJ, Chowdhry S, Sharma RS, Ashford FB, Walsh SV, McCrimmon RJ, et al. Susceptibility of Nrf2-null mice to steatohepatitis and cirrhosis upon consumption of a high-fat diet is associated with oxidative stress, perturbation of the unfolded protein response, and disturbance in the expression of metabolic enzymes but not with insulin resistance. *Mol Cell Biol.* 2014;34(17):3305-20.
37. Li L, Fu J, Liu D, Sun J, Hou Y, Chen C, et al. Hepatocyte-specific Nrf2 deficiency mitigates high-fat diet-induced hepatic steatosis: Involvement of reduced PPARgamma expression. *Redox Biol.* 2020;30:101412.
38. Chartoumpekis DV, Palliyaguru DL, Wakabayashi N, Fazzari M, Khoo NKH, Schopfer FJ, et al. Nrf2 deletion from adipocytes, but not hepatocytes, potentiates systemic metabolic dysfunction after long-term high-fat diet-induced obesity in mice. *Am J Physiol Endocrinol Metab.* 2018;315(2):E180-E95.
39. More VR, Xu JL, Shimpi PC, Belgrave C, Luyendyk JP, Yamamoto M, et al. Keap1 knockdown increases markers of metabolic syndrome after long-term high fat diet feeding. *Free Radical Bio Med.* 2013;61:85-94.
40. Zhang YK, Yeager RL, Tanaka Y, and Klaassen CD. Enhanced expression of Nrf2 in mice attenuates the fatty liver produced by a methionine- and choline-deficient diet. *Toxicol Appl Pharmacol.* 2010;245(3):326-34.
41. Hoang SA, Oseini A, Feaver RE, Cole BK, Asgharpour A, Vincent R, et al. Gene Expression Predicts Histological Severity and Reveals Distinct Molecular Profiles of Nonalcoholic Fatty Liver Disease. *Sci Rep.* 2019;9(1):12541.
42. Pendyala S, Moitra J, Kalari S, Kleeberger SR, Zhao Y, Reddy SP, et al. Nrf2 regulates hyperoxia-induced Nox4 expression in human lung endothelium: identification of functional antioxidant response elements on the Nox4 promoter. *Free Radic Biol Med.* 2011;50(12):1749-59.
43. Fisher-Wellman KH, and Neufer PD. Linking mitochondrial bioenergetics to insulin resistance via redox biology. *Trends Endocrinol Metab.* 2011;23(3):142-53.
44. Xirouchaki CE, Jia Y, McGrath MJ, Greatorex S, Tran M, Merry TL, et al. Skeletal muscle NOX4 is required for adaptive responses that prevent insulin resistance. *Sci Adv.* 2021;7(51):eabl4988.
45. Kuroda J, Ago T, Matsushima S, Zhai P, Schneider MD, and Sadoshima J. NADPH oxidase 4 (Nox4) is a major source of oxidative stress in the failing heart. *Proc Natl Acad Sci USA.* 2010;107(35):15565-70.
46. Aoyama T, Paik YH, Watanabe S, Laleu B, Gaggini F, Fioraso-Cartier L, et al. Nicotinamide adenine dinucleotide phosphate oxidase in experimental liver fibrosis: GKT137831 as a novel potential therapeutic agent. *Hepatology.* 2012;56(6):2316-27.
47. Flekac M, Skrha J, Hilgertova J, Lacinova Z, and Jarolimkova M. Gene polymorphisms of superoxide dismutases and catalase in diabetes mellitus. *BMC Med Genet.* 2008;9:30.
48. Loor G, Kondapalli J, Schriewer JM, Chandel NS, Vanden Hoek TL, and Schumacker PT. Menadione triggers cell death through ROS-dependent mechanisms involving

PARP activation without requiring apoptosis. *Free Radical Bio Med.* 2010;49(12):1925-36.
49. Blaser H, Dostert C, Mak TW, and Brenner D. TNF and ROS Crosstalk in Inflammation. *Trends Cell Biol.* 2016;26(4):249-61.
50. Hwang S, Wang X, Rodrigues RM, Ma J, He Y, Seo W, et al. Protective and Detrimental Roles of p38alpha Mitogen-Activated Protein Kinase in Different Stages of Nonalcoholic Fatty Liver Disease. *Hepatology.* 2020;72(3):873-91.
51. Tanaka Y, Aleksunes LM, Yeager RL, Gyamfi MA, Esterly N, Guo GL, et al. NF-E2-related factor 2 inhibits lipid accumulation and oxidative stress in mice fed a high-fat diet. *J Pharmacol Exp Ther.* 2008;325(2):655-64.
52. Yates MS, Tran QT, Dolan PM, Osburn WO, Shin S, McCulloch CC, et al. Genetic versus chemoprotective activation of Nrf2 signaling: overlapping yet distinct gene expression profiles between Keap1 knockout and triterpenoid-treated mice. *Carcinogenesis.* 2009;30(6):1024-31.
53. Kay HY, Kim WD, Hwang SJ, Choi HS, Gilroy RK, Wan YJ, et al. Nrf2 inhibits LXRalpha-dependent hepatic lipogenesis by competing with FXR for acetylase binding. *Antioxid Redox Signal.* 2011;15(8):2135-46.
54. Wolf MJ, Adili A, Piotrowitz K, Abdullah Z, Boege Y, Stemmer K, et al. Metabolic activation of intrahepatic CD8+ T cells and NKT cells causes nonalcoholic steatohepatitis and liver cancer via cross-talk with hepatocytes. *Cancer Cell.* 2014;26(4):549-64.
55. Haas JT, Vonghia L, Mogilenko DA, Verrijken A, Molendi-Coste O, Fleury S, et al. Transcriptional Network Analysis Implicates Altered Hepatic Immune Function in NASH development and resolution. *Nat Metab.* 2019;1(6):604-14.
56. Sutti S, and Albano E. Adaptive immunity: an emerging player in the progression of NAFLD. *Nat Rev Gastroenterol Hepatol.* 2020;17(2):81-92.
57. Dudek M, Pfister D, Donakonda S, Filpe P, Schneider A, Laschinger M, et al. Auto-aggressive CXCR6(+) CD8 T cells cause liver immune pathology in NASH. *Nature.* 2021;592(7854):444-9.
58. Kiourtis C, Wilczynska A, Nixon C, Clark W, May S, and Bird TG. Specificity and off-target effects of AAV8-TBG viral vectors for the manipulation of hepatocellular gene expression in mice. *Biol Open.* 2021;10(9).
59. Loft A, Alfaro AJ, Schmidt SF, Pedersen FB, Terkelsen MK, Puglia M, et al. Liver-fibrosis-activated transcriptional networks govern hepatocyte reprogramming and intra-hepatic communication. *Cell Metab.* 2021;33(8):1685-700.
60. Sies H, and Jones DP. Reactive oxygen species (ROS) as pleiotropic physiological signalling agents. *Nat Rev Mol Cell Biol.* 2020;21(7):363-83.
61. Houstis N, Rosen ED, and Lander ES. Reactive oxygen species have a causal role in multiple forms of insulin resistance. *Nature.* 2006;440(7086):944-8.
62. Furukawa S, Fujita T, Shimabukuro M, Iwaki M, Yamada Y, Nakajima Y, et al. Increased oxidative stress in obesity and its impact on metabolic syndrome. *J Clin Invest.* 2004;114(12):1752-61.
63. Tiganis T. Reactive oxygen species and insulin resistance: the good, the bad and the ugly. *Trends Pharmacol Sci.* 2011;32(2):82-9.
64. Hancock M, Hafstad AD, Nabeebaccus AA, Catibog N, Logan A, Smyrnias I, et al. Myocardial NADPH oxidase-4 regulates the physiological response to acute exercise. *eLife.* 2018;7.
65. Ristow M, Zarse K, Oberbach A, Kloting N, Birringer M, Kiehntopf M, et al. Antioxidants prevent health-promoting effects of physical exercise in humans. *Proc Natl Acad Sci USA.* 2009;106(21):8665-70.

66. Carter CS, Huang SC, Searby CC, Cassaidy B, Miller MJ, Grzesik WJ, et al. Exposure to Static Magnetic and Electric Fields Treats Type 2 Diabetes. *Cell Metab.* 2020;32(4):561-74.
67. Merry TL, Tran M, Dodd GT, Mangiafico SP, Wiede F, Kaur S, et al. Hepatocyte glutathione peroxidase-1 deficiency improves hepatic glucose metabolism and decreases steatohepatitis in mice. *Diabetologia.* 2016;59(12):2632-44.
68. Nobili V, Donati B, Panera N, Vongsakulyanon A, Alisi A, Dallapiccola B, et al. A 4-polymorphism risk score predicts steatohepatitis in children with nonalcoholic fatty liver disease. *J Pediatr Gastroenterol Nutr.* 2014;58(5):632-6.
69. Jiang JX, Chen X, Serizawa N, Szyndralewiez C, Page P, Schroder K, et al. Liver fibrosis and hepatocyte apoptosis are attenuated by GKT137831, a novel NOX4/NOX1 inhibitor in vivo. *Free Radic Biol Med.* 2012;53(2):289-96.
70. Lan T, Kisseleva T, and Brenner DA. Deficiency of NOX1 or NOX4 Prevents Liver Inflammation and Fibrosis in Mice through Inhibition of Hepatic Stellate Cell Activation. *Plos One.* 2015;10(7).
71. Gornicka A, Morris-Stiff G, Thapaliya S, Papouchado BG, Berk M, and Feldstein AE. Transcriptional profile of genes involved in oxidative stress and antioxidant defense in a dietary murine model of steatohepatitis. *Antioxid Redox Signal.* 2011;15(2):437-45.
72. Moore MP, Cunningham RP, Meers GM, Johnson SA, Wheeler AA, Ganga RR, et al. Compromised hepatic mitochondrial fatty acid oxidation and reduced markers of mitochondrial turnover in human NAFLD. *Hepatology.* 2022; 76(5):1452-1465.

ACKNOWLEDGMENTS

We thank the Monash Metabolic Phenotyping Platform for assistance with clamps. This work was supported by Diabetes Australia and the National Health and Medical Research Council of Australia (to T.T.).

AUTHOR CONTRIBUTIONS

T.T. conceived/conceptualized the study, designed experiments, wrote the manuscript and interpreted the data with intellectual input from all authors. S.G. S.K. and C.E.X. conceptualized and designed experiments, conducted and analysed experiments and contributed to manuscript reviewing/editing. Other authors performed and/or analysed experiments and/or contributed to manuscript reviewing/editing.

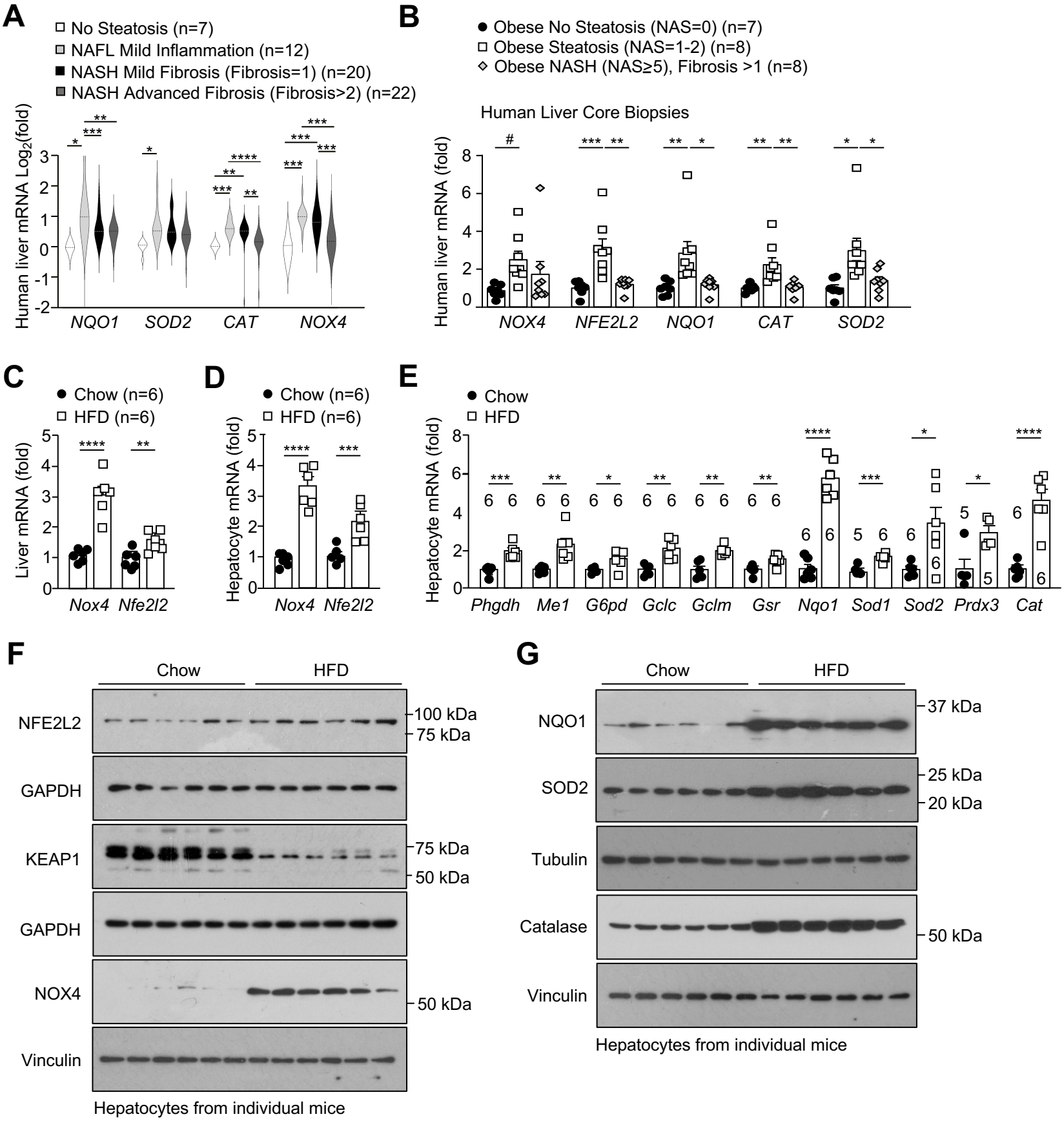
A
No Steatosis (n=7)
NAFL Mild Inflammation (n=12)
NASH Mild Fibrosis (Fibrosis=1) (n=20)
NASH Advanced Fibrosis (Fibrosis>2) (n=22)
Human liver mRNA Log2(fold)
NQO1
SOD2
CAT
NOX4
B
Obese No Steatosis (NAS=0) (n=7)
Obese Steatosis (NAS=1-2) (n=8)
Obese NASH (NAS≥5), Fibrosis >1 (n=8)
Human Liver Core Biopsies
Human liver mRNA (fold)
NOX4
NFE2L2
NQO1
CAT
SOD2
C
Chow (n=6)
HFD (n=6)
Liver mRNA (fold)
Nox4
Nfe2l2
D
Chow (n=6)
HFD (n=6)
Hepatocyte mRNA (fold)
Nox4
Nfe2l2
E
Chow
HFD
Hepatocyte mRNA (fold)
Phgdh
Me1
G6pd
Gclc
Gclm
Gsr
Nqo1
Sod1
Sod2
Prdx3
Cat
F
Chow
HFD
NFE2L2
100 kDa
75 kDa
GAPDH
KEAP1
75 kDa
50 kDa
GAPDH
NOX4
50 kDa
Vinculin
Hepatocytes from individual mice
G
Chow
HFD
NQO1
37 kDa
SOD2
25 kDa
20 kDa
Tubulin
Catalase
50 kDa
Vinculin
Hepatocytes from individual mice
H
Chow (n=6)
HFD (n=6)
Protein (fold)
NFE2L2
KEAP1
NOX4
NQO1
SOD2
CAT

FIG 1

Figure 1. NOX4 and NFE2L2 antioxidant defense gene expression in NAFLD. **a)** RNAseq analysis (GSE130970) of livers from patients without steatosis (n=7), with NAFL (n=13; NAS=1-4, fibrosis score=0), NASH with mild fibrosis (n= 20; NAS=3-6, fibrosis score=1), or NASH with advanced fibrosis (n=22; NAS=3-6, fibrosis score ≥2). **b)** qPCR analysis of liver core biopsies from obese patients without steatosis (n=7; NAS=0), with NAFL (n=8; NAS=1-2) or NASH and fibrosis (n=8; NAS >5, fibrosis score=1-2). **c**) C57BL/6 mice were fed a chow-diet or a HFD for 12-weeks and livers processed for qPCR. **d-h**) C57BL/6 mice were fed a chow-diet or HFD for 8-10-weeks and hepatocytes isolated and processed for **d-e)** qPCR or **f-g)** immunoblotting. **h)** Quantification of protein from f-g. Representative and quantified results are shown (mean±SEM) for the indicated number of mice. Significance determined using (c-e, h) Student's t-test, or (a-b) one-way ANOVA.

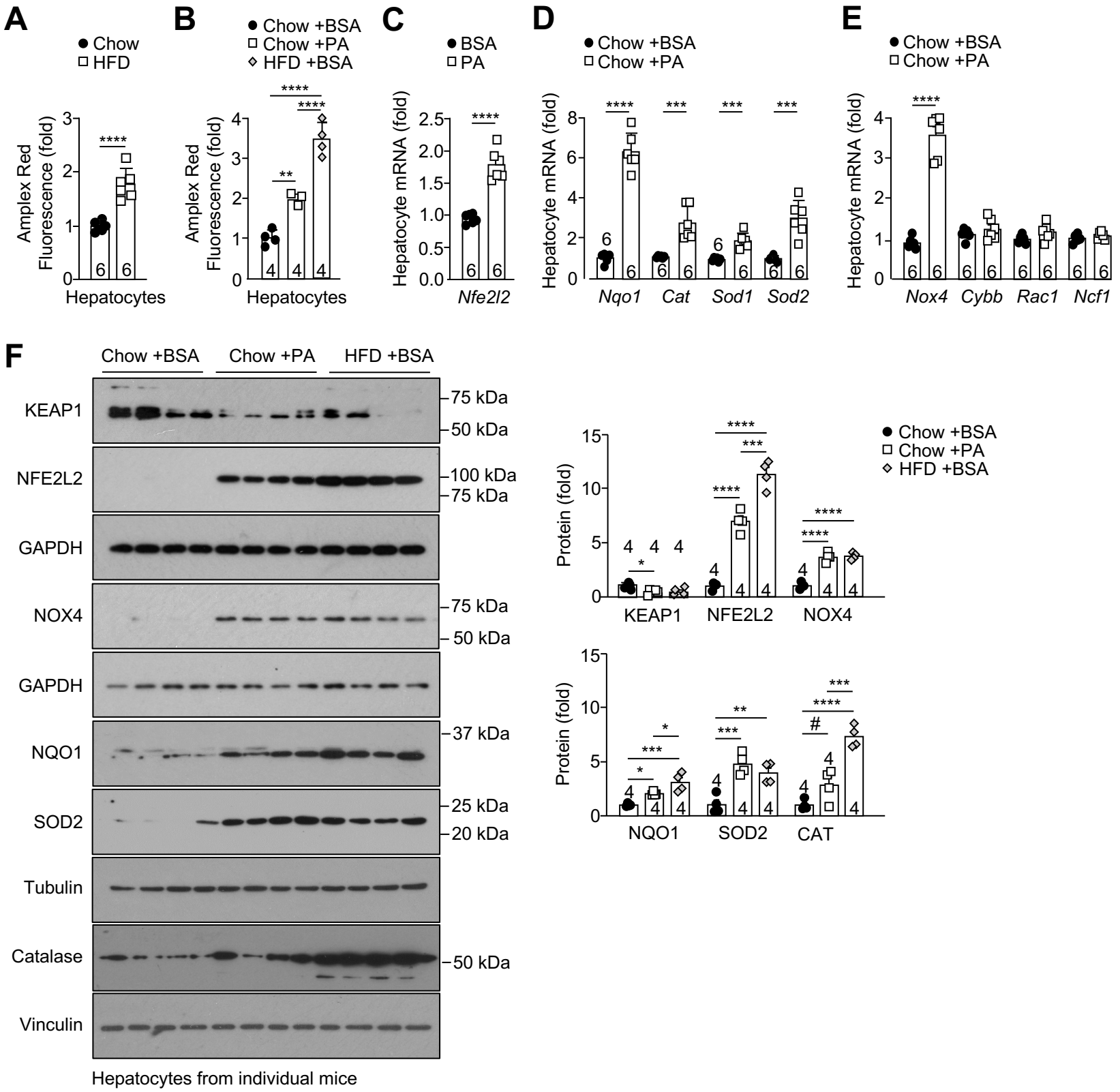
A
Chow
HFD
Amplex Red Fluorescence (fold)
Hepatocytes
B
Chow +BSA
Chow +PA
HFD +BSA
Amplex Red Fluorescence (fold)
Hepatocytes
C
BSA
PA
Hepatocyte mRNA (fold)
Nfe2l2
D
Chow +BSA
Chow +PA
Hepatocyte mRNA (fold)
Nqo1
Cat
Sod1
Sod2
E
Chow +BSA
Chow +PA
Hepatocyte mRNA (fold)
Nox4
Cybb
Rac1
Ncf1
F
Chow +BSA
Chow +PA
HFD +BSA
KEAP1
NFE2L2
GAPDH
NOX4
GAPDH
NQO1
SOD2
Tubulin
75 kDa
50 kDa
100 kDa
75 kDa
75 kDa
50 kDa
37 kDa
25 kDa
20 kDa
Protein (fold)
KEAP1
NFE2L2
NOX4
NQO1
SOD2
CAT
Catalase
Vinculin
50 kDa
Hepatocytes from individual mice
G
Chow +BSA
Chow +PA
Chow +PA +MitoT
Amplex Red Fluorescence (Fold)
Hepatocytes
H
Chow +BSA
Chow +PA
Chow +PA + MitoT
Hepatocyte mRNA (fold)
Nfe2l2
Nox4
Cat
Nqo1
Sod1
Sod2

FIG 2

Figure 2. Lipids and mitochondrial ROS drive antioxidant defense. **a-b)** C57BL/6 mice were fed a chow-diet and/or a HFD for 8-10-weeks and hepatocytes isolated, cultured for 16h and **a**) processed for extracellular H_2O_2 measurements using Amplex Red, or **b**) treated with BSA-conjugated palmitate (PA) or BSA for 16h and processed for H_2O_2 measurements, or **c-e)** processed for qPCR, or **f**) treated with BSA or PA for 36h and processed for immunoblotting, or **g-h)** treated with BSA, PA or PA plus 20 μM mitoTEMPOL (MitoT) for 16h and processed for qPCR. Representative and quantified results are shown (mean±SEM) for the indicated number of mice. Significance determined using (a, c-e) Student's t-test, or (b, f-h) one-way ANOVA; # Student's t-test.

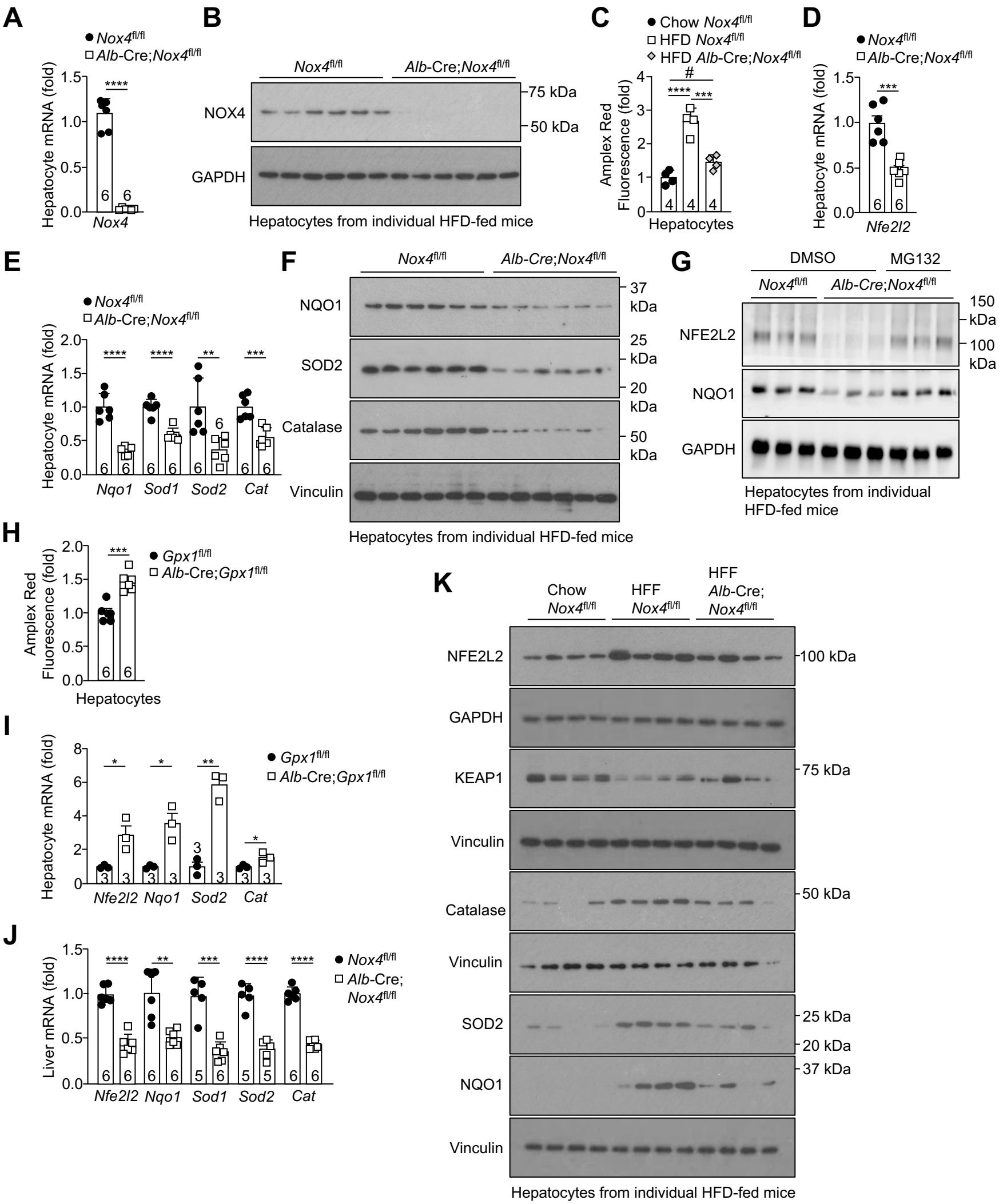
A
Nox4fl/fl
Alb-Cre;Nox4fl/fl
Hepatocyte mRNA (fold)
Nox4
B
Nox4fl/fl
Alb-Cre;Nox4fl/fl
NOX4
GAPDH
75 kDa
50 kDa
Hepatocytes from individual HFD-fed mice
C
Chow Nox4fl/fl
HFD Nox4fl/fl
HFD Alb-Cre;Nox4fl/fl
Amplex Red Fluorescence (fold)
Hepatocytes
D
Nox4fl/fl
Alb-Cre;Nox4fl/fl
Hepatocyte mRNA (fold)
Nfe2l2
E
Nox4fl/fl
Alb-Cre;Nox4fl/fl
Hepatocyte mRNA (fold)
Nqo1
Sod1
Sod2
Cat
F
Nox4fl/fl
Alb-Cre;Nox4fl/fl
NQO1
SOD2
Catalase
Vinculin
37 kDa
25 kDa
20 kDa
50 kDa
Hepatocytes from individual HFD-fed mice
G
DMSO
MG132
Nox4fl/fl
Alb-Cre;Nox4fl/fl
NFE2L2
NQO1
GAPDH
150 kDa
100 kDa
Hepatocytes from individual HFD-fed mice
H
Gpx1fl/fl
Alb-Cre;Gpx1fl/fl
Amplex Red Fluorescence (fold)
Hepatocytes
I
Gpx1fl/fl
Alb-Cre;Gpx1fl/fl
Hepatocyte mRNA (fold)
Nfe2l2
Nqo1
Sod2
Cat
J
Nox4fl/fl
Alb-Cre; Nox4fl/fl
Liver mRNA (fold)
Nfe2l2
Nqo1
Sod1
Sod2
Cat
K
Chow Nox4fl/fl
HFF Nox4fl/fl
HFF Alb-Cre; Nox4fl/fl
NFE2L2
GAPDH
KEAP1
Vinculin
Catalase
Vinculin
SOD2
NQO1
Vinculin
100 kDa
75 kDa
50 kDa
25 kDa
20 kDa
37 kDa
Hepatocytes from individual HFD-fed mice

FIG 3

Figure 3. NOX4 is essential for antioxidant defense. **a-b)** *Nox4*$^{fl/fl}$ or *Alb*-Cre;*Nox4*$^{fl/fl}$ mice were fed a HFD for 8-10-weeks and hepatocytes isolated and processed for **a)** qPCR, or **b)** immunoblotting to assess NOX4 expression. **c)** C57BL/6 mice were fed a chow-diet or HFD and hepatocytes isolated and processed for H_2O_2 measurements. **d-f**) *Nox4*$^{fl/fl}$ or *Alb*-Cre;*Nox4*$^{fl/fl}$ mice were fed a HFD and hepatocytes isolated and processed for **d-e**) qPCR or **f**) immunoblotting. **g**) *Nox4*$^{fl/fl}$ or *Alb*-Cre;*Nox4*$^{fl/fl}$ mice were fed a HFD and hepatocytes incubated with vehicle or MG132 for 36h and processed for immunoblotting. **h-i**) Hepatocytes were isolated from chow-fed *Gpx1*$^{fl/fl}$ or *Alb*-Cre;*Gpx1*$^{fl/fl}$ (C57BL/6) mice and processed for **h**) H_2O_2 measurements, or **i**) qPCR. **j**) *Nox4*$^{fl/fl}$ or *Alb*-Cre;*Nox4*$^{fl/fl}$ mice were fed a HFD for 12-weeks and livers processed for qPCR. **k**) *Nox4*$^{fl/fl}$ or *Alb*-Cre;*Nox4*$^{fl/fl}$ mice were fed a chow-diet or HFD and hepatocytes isolated and processed for immunoblotting. Representative and quantified results are shown (mean±SEM) for the indicated number of mice. Significance determined using (a, d,e, h-j) Student's t-test or (c) one-way ANOVA; # Student's t-test.

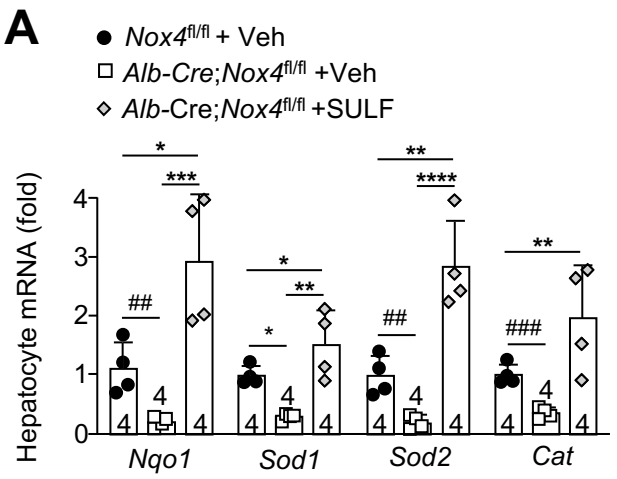
A
Nox4fl/fl + Veh
Alb-Cre;Nox4fl/fl +Veh
Alb-Cre;Nox4fl/fl +SULF
Hepatocyte mRNA (fold)
Nqo1
Sod1
Sod2
Cat

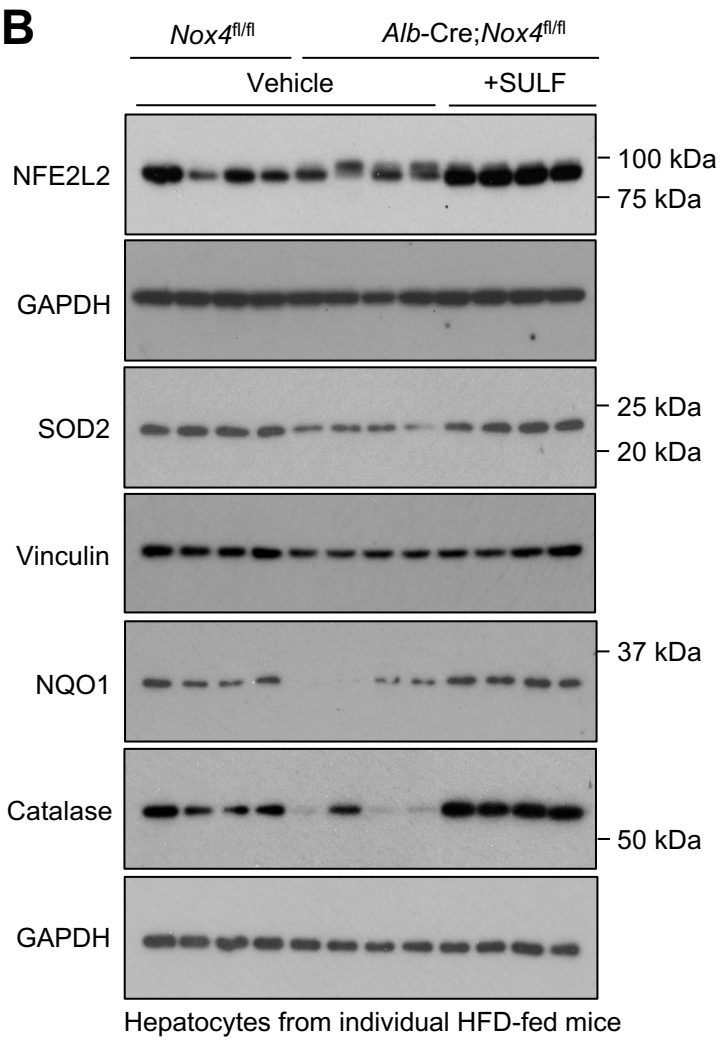
B
Nox4fl/fl
Alb-Cre;Nox4fl/fl
Vehicle
+SULF
NFE2L2
GAPDH
SOD2
Vinculin
NQO1
Catalase
GAPDH
100 kDa
75 kDa
25 kDa
20 kDa
37 kDa
50 kDa
Hepatocytes from individual HFD-fed mice

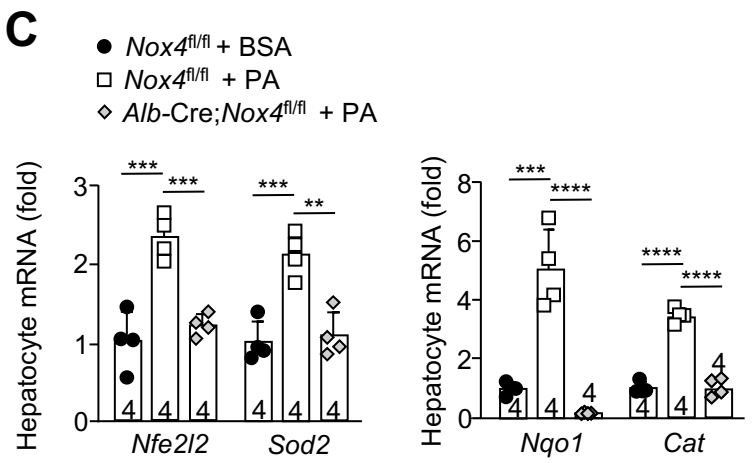
C
Nox4fl/fl + BSA
Nox4fl/fl + PA
Alb-Cre;Nox4fl/fl + PA
Hepatocyte mRNA (fold)
Nfe2l2
Sod2
Nqo1
Cat

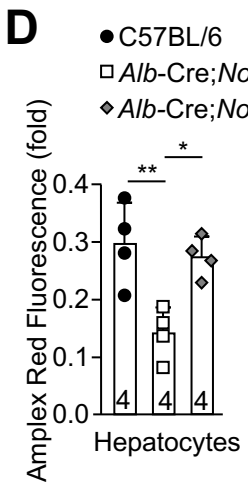
D
C57BL/6
Alb-Cre;Nox4fl/fl
Alb-Cre;Nox4fl/fl;Gpx1fl/fl
Amplex Red Fluorescence (fold)
Hepatocytes

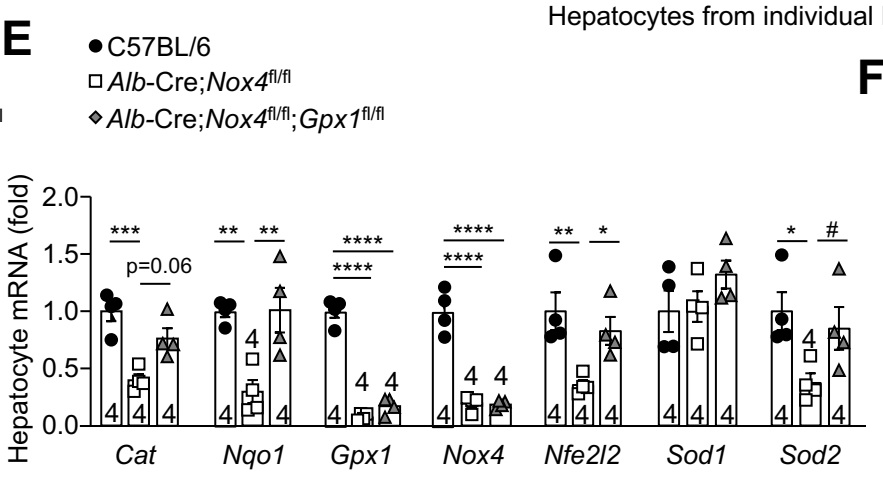
E
C57BL/6
Alb-Cre;Nox4fl/fl
Alb-Cre;Nox4fl/fl;Gpx1fl/fl
Hepatocyte mRNA (fold)
p=0.06
Cat
Nqo1
Gpx1
Nox4
Nfe2l2
Sod1
Sod2

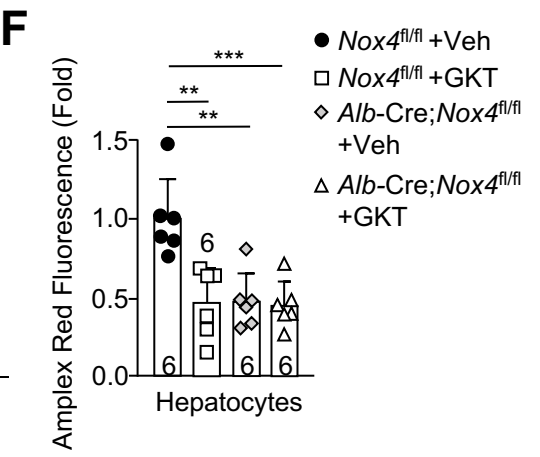
F
Nox4fl/fl +Veh
Nox4fl/fl +GKT
Alb-Cre;Nox4fl/fl +Veh
Alb-Cre;Nox4fl/fl +GKT
Amplex Red Fluorescence (Fold)
Hepatocytes

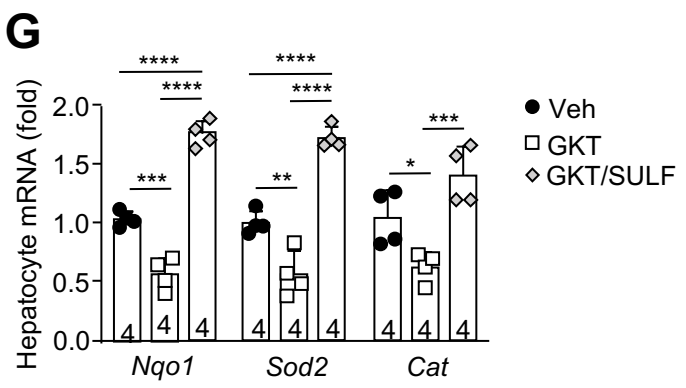
G
Veh
GKT
GKT/SULF
Hepatocyte mRNA (fold)
Nqo1
Sod2
Cat

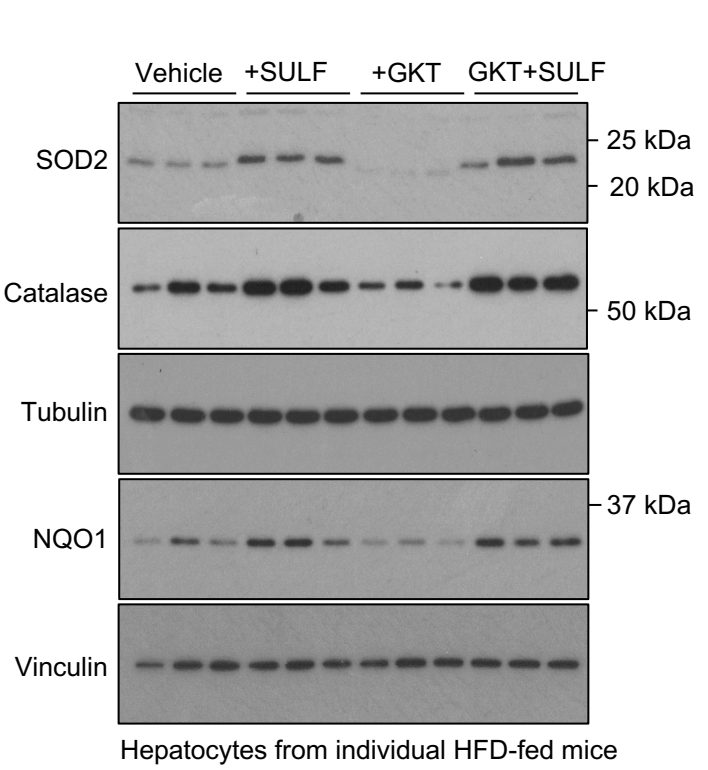
H
Vehicle
+SULF
+GKT
GKT+SULF
SOD2
Catalase
Tubulin
NQO1
Vinculin
25 kDa
20 kDa
50 kDa
37 kDa
Hepatocytes from individual HFD-fed mice

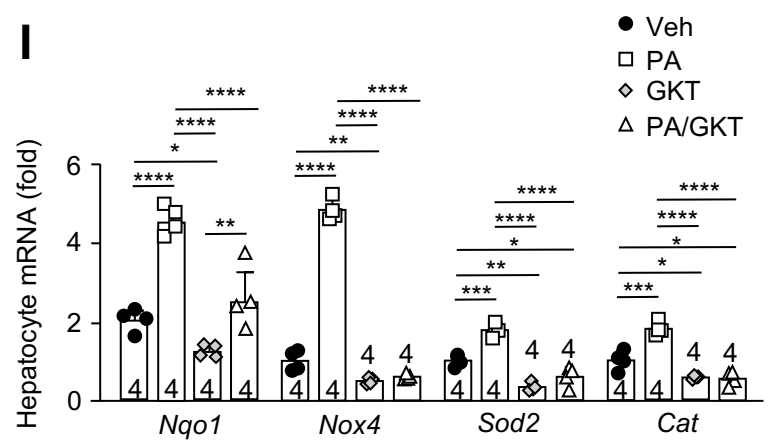
I
Veh
PA
GKT
PA/GKT
Hepatocyte mRNA (fold)
Nqo1
Nox4
Sod2
Cat

FIG 4

Figure 4. NOX4-derived H_2O_2 is essential for antioxidant defense. **a-b**) *Nox4*$^{fl/fl}$ or *Alb*-Cre;*Nox4*$^{fl/fl}$ mice were fed a HFD for 8-10-weeks and hepatocytes isolated and treated with vehicle (DMSO) or 1 μM sulforaphane (SULF) for **a**) 16h and processed for qPCR, or **b**) 36h and processed for immunoblotting. **c**) Alternatively, hepatocytes were treated with BSA or PA for 16h and processed for qPCR. **d-e**) 8-week-old *Nox4*$^{fl/fl}$, *Alb*-Cre;*Nox4*$^{fl/fl}$ or *Alb*-Cre;*Nox4*$^{fl/fl}$;*Gpx1*$^{fl/fl}$ mice were fed a HFD for 8-10-weeks and hepatocytes isolated and processed for **d**) H_2O_2 measurements, or **e**) qPCR. **f-h**) *Nox4*$^{fl/fl}$ or *Alb*-Cre;*Nox4*$^{fl/fl}$ mice were fed a HFD for 8-10-weeks and isolated hepatocytes treated with vehicle (DMSO), 40 μM GKT137831 (GKT), or GKT plus 1 μM SULF for 16h and processed for **f**) H_2O_2 measurements and **g**) qPCR, or **h**) 36h and processed for immunoblotting. **i**) Alternatively, hepatocytes were treated with vehicle, PA, GKT or PA plus GKT for 16h and processed for qPCR. Representative and quantified results are shown (mean±SEM) for the indicated number of mice. Significance determined using (a, i) Student's t-test or (a, c, d, e, g) one-way ANOVA or (f, i) two-way ANOVA; # Student's t-test.

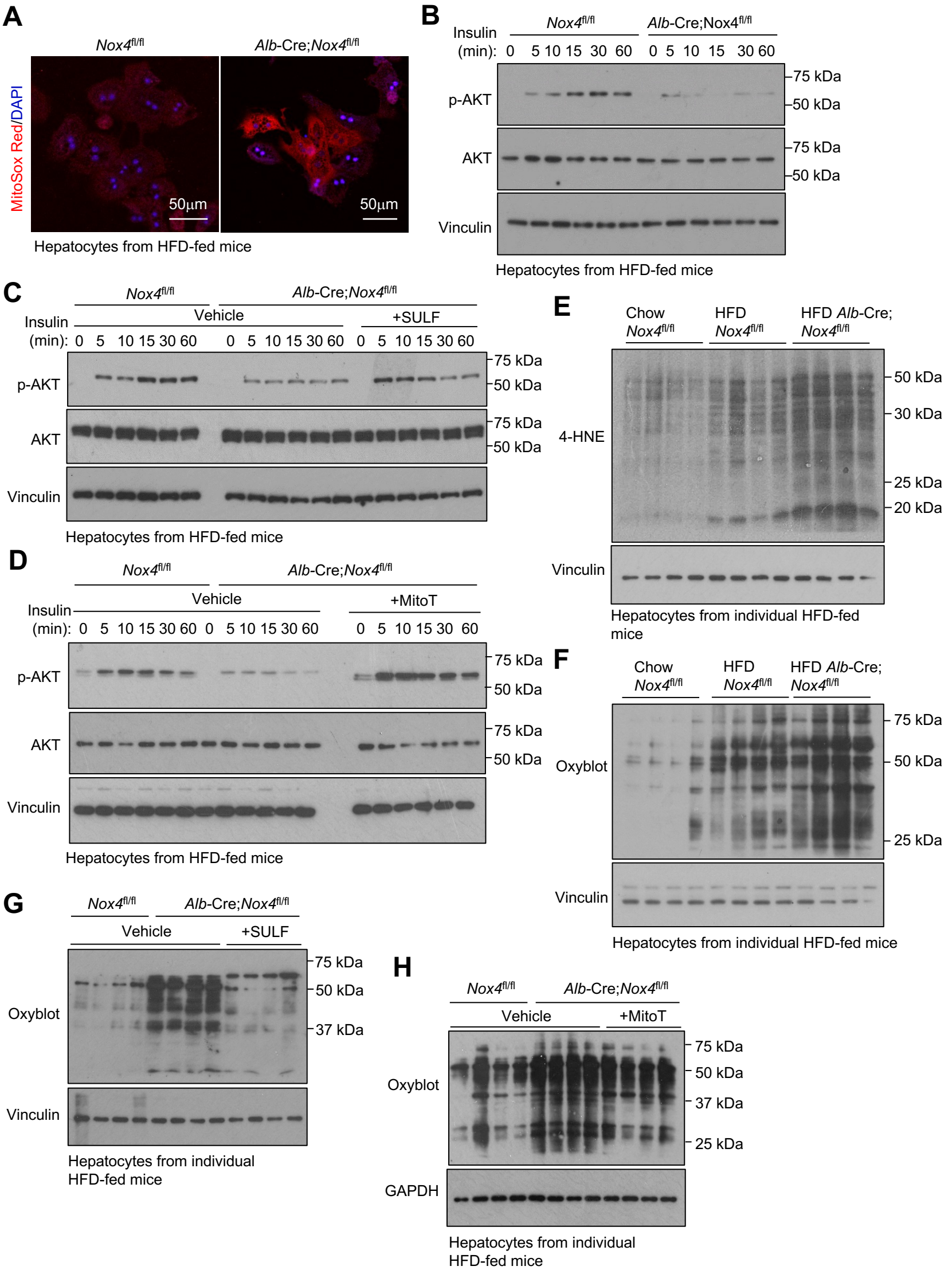
A
Nox4fl/fl
Alb-Cre;Nox4fl/fl
MitoSox Red/DAPI
50μm
50μm
Hepatocytes from HFD-fed mice
B
Insulin
(min): 0 5 10 15 30 60 0 5 10 15 30 60
Nox4fl/fl
Alb-Cre;Nox4fl/fl
p-AKT
AKT
Vinculin
75 kDa
50 kDa
75 kDa
50 kDa
Hepatocytes from HFD-fed mice
C
Nox4fl/fl
Alb-Cre;Nox4fl/fl
Vehicle
+SULF
Insulin
(min): 0 5 10 15 30 60 0 5 10 15 30 60 0 5 10 15 30 60
p-AKT
AKT
Vinculin
75 kDa
50 kDa
75 kDa
50 kDa
Hepatocytes from HFD-fed mice
D
Nox4fl/fl
Alb-Cre;Nox4fl/fl
Vehicle
+MitoT
Insulin
(min): 0 5 10 15 30 60 0 5 10 15 30 60 0 5 10 15 30 60
p-AKT
AKT
Vinculin
75 kDa
50 kDa
75 kDa
50 kDa
Hepatocytes from HFD-fed mice
E
Chow
Nox4fl/fl
HFD
Nox4fl/fl
HFD Alb-Cre;
Nox4fl/fl
4-HNE
Vinculin
50 kDa
30 kDa
25 kDa
20 kDa
Hepatocytes from individual HFD-fed mice
F
Chow
Nox4fl/fl
HFD
Nox4fl/fl
HFD Alb-Cre;
Nox4fl/fl
Oxyblot
Vinculin
75 kDa
50 kDa
25 kDa
Hepatocytes from individual HFD-fed mice
G
Nox4fl/fl
Alb-Cre;Nox4fl/fl
Vehicle
+SULF
Oxyblot
Vinculin
75 kDa
50 kDa
37 kDa
Hepatocytes from individual
HFD-fed mice
H
Nox4fl/fl
Alb-Cre;Nox4fl/fl
Vehicle
+MitoT
Oxyblot
GAPDH
75 kDa
50 kDa
37 kDa
25 kDa
Hepatocytes from individual
HFD-fed mice

FIG 5

Figure 5. NOX4 deletion in hepatocytes promotes oxidative stress and insulin resistance. **a-b)** *Nox4*$^{fl/fl}$ or *Alb*-Cre;*Nox4*$^{fl/fl}$ mice were fed a HFD for 8-10-weeks and isolated hepatocytes either **a**) stained with 1 μM MitoSOX™ Red and analysed by confocal microscopy (counterstained with DAPI) or **b**) serum-starved and stimulated with 1 nM insulin and processed for immunoblotting to monitor for AKT Ser-473 phosphorylation (p-AKT). **c-d**) Alternatively hepatocytes were treated with vehicle, 1 μM SULF or 20 μM MitoT for 16h, serum-starved, and then stimulated with 1 nM insulin and processed for immunoblotting. **e-f)** *Nox4*$^{fl/fl}$ or *Alb*-Cre;*Nox4*$^{fl/fl}$ mice were fed a chow-diet or HFD for 8-10-weeks and hepatocytes isolated and processed for lipid peroxidation (4-HNE) or protein carbonylation (Oxyblot) analysis by immunoblotting. **g-h**) *Nox4*$^{fl/fl}$ or *Alb*-Cre;*Nox4*$^{fl/fl}$ mice were fed a HFD for 8-10-weeks and isolated hepatocytes treated with vehicle, 1 μM SULF or 20 μM MitoT for 16h and processed for 4-HNE or Oxyblot immunoblotting. Representative results of at least three independent experiments are shown.

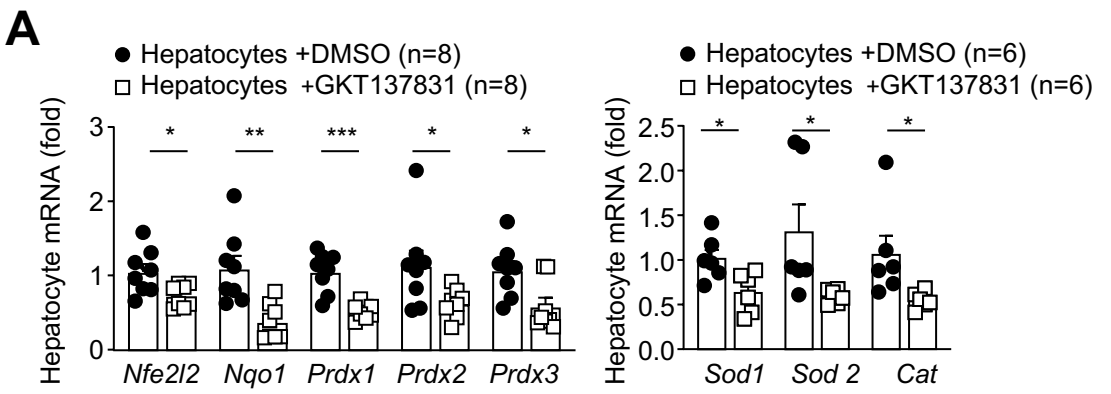
A
Hepatocytes +DMSO (n=8)
Hepatocytes +GKT137831 (n=8)
Hepatocyte mRNA (fold)
Nfe2l2
Nqo1
Prdx1
Prdx2
Prdx3
Hepatocytes +DMSO (n=6)
Hepatocytes +GKT137831 (n=6)
Hepatocyte mRNA (fold)
Sod1
Sod 2
Cat

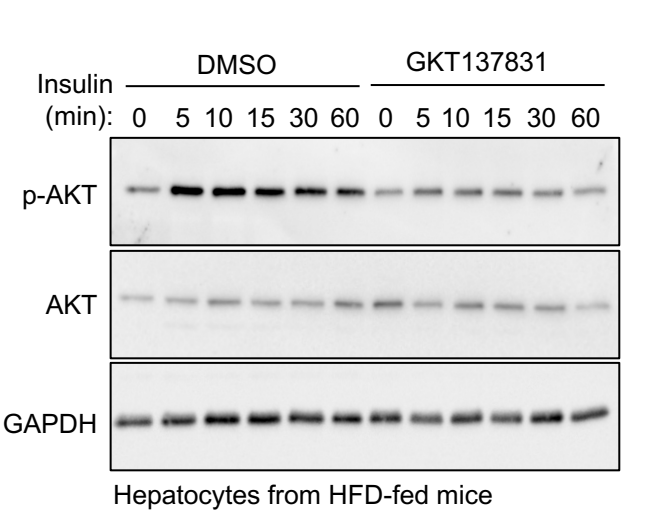
B
Insulin
DMSO
GKT137831
(min): 0 5 10 15 30 60 0 5 10 15 30 60
p-AKT
AKT
GAPDH
Hepatocytes from HFD-fed mice

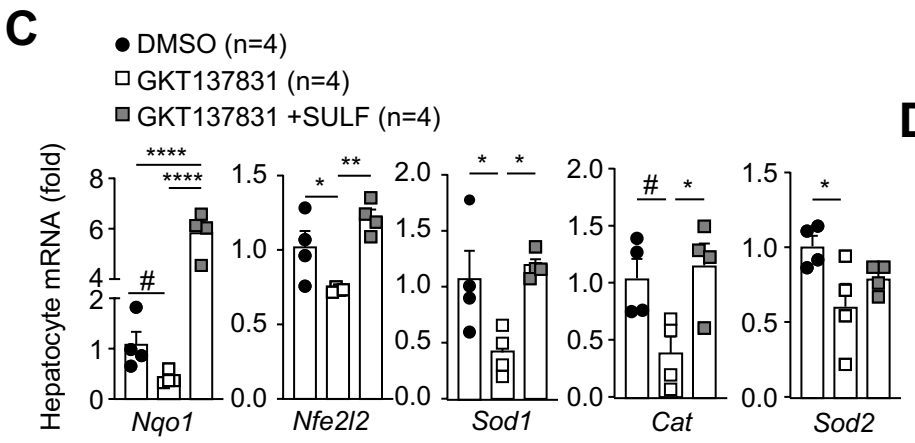
C
DMSO (n=4)
GKT137831 (n=4)
GKT137831 +SULF (n=4)
Hepatocyte mRNA (fold)
Nqo1
Nfe2l2
Sod1
Cat
Sod2

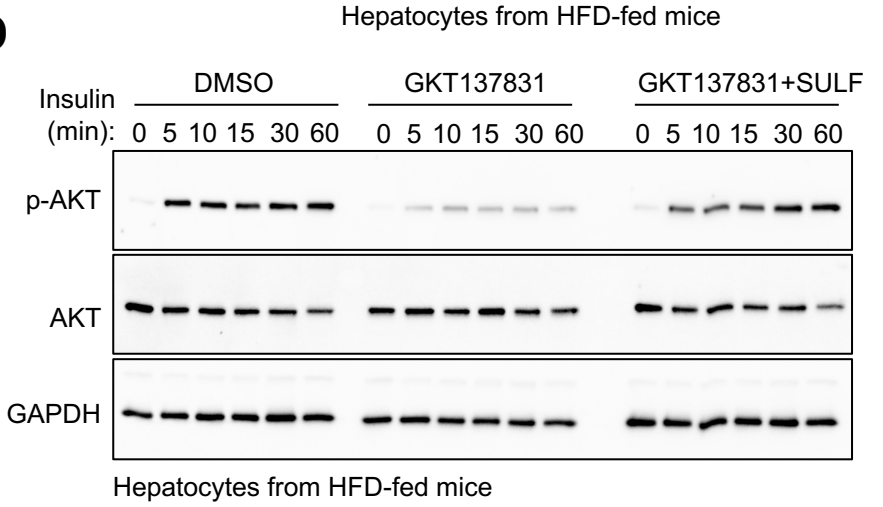
D
Insulin
DMSO
GKT137831
GKT137831+SULF
(min): 0 5 10 15 30 60 0 5 10 15 30 60 0 5 10 15 30 60
p-AKT
AKT
GAPDH
Hepatocytes from HFD-fed mice

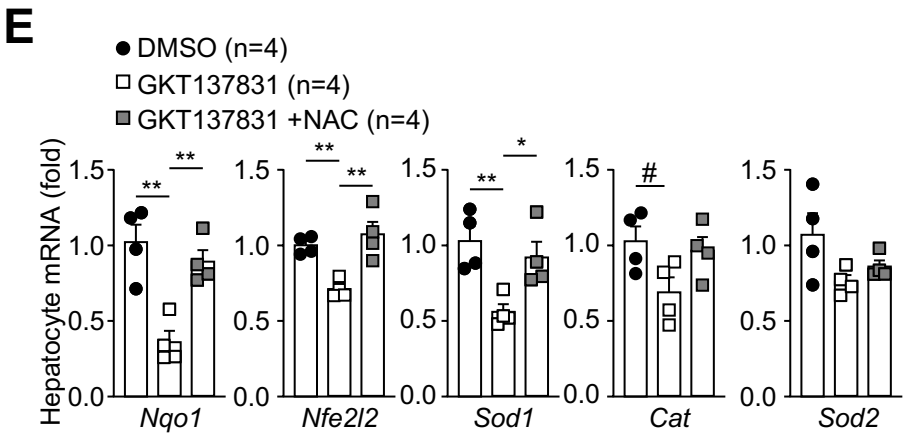
E
DMSO (n=4)
GKT137831 (n=4)
GKT137831 +NAC (n=4)
Hepatocyte mRNA (fold)
Nqo1
Nfe2l2
Sod1
Cat
Sod2

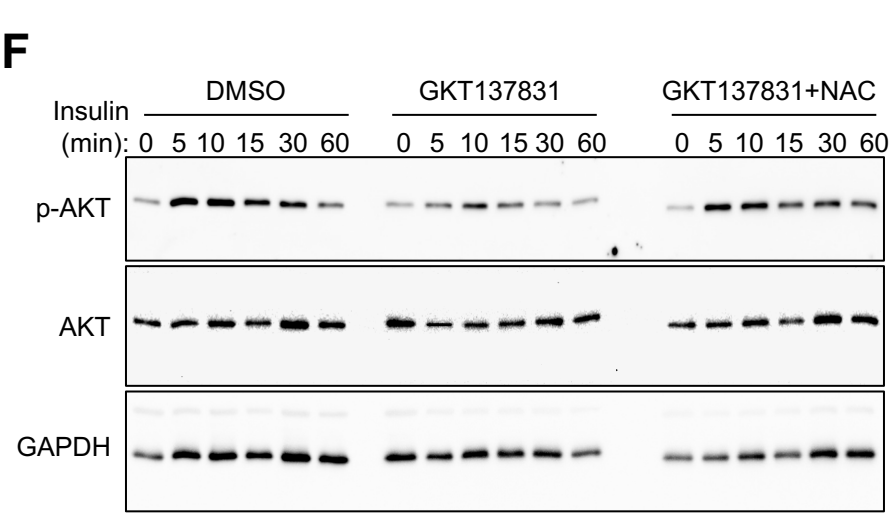
F
Insulin
DMSO
GKT137831
GKT137831+NAC
(min): 0 5 10 15 30 60 0 5 10 15 30 60 0 5 10 15 30 60
p-AKT
AKT
GAPDH
Hepatocytes from HFD-fed mice

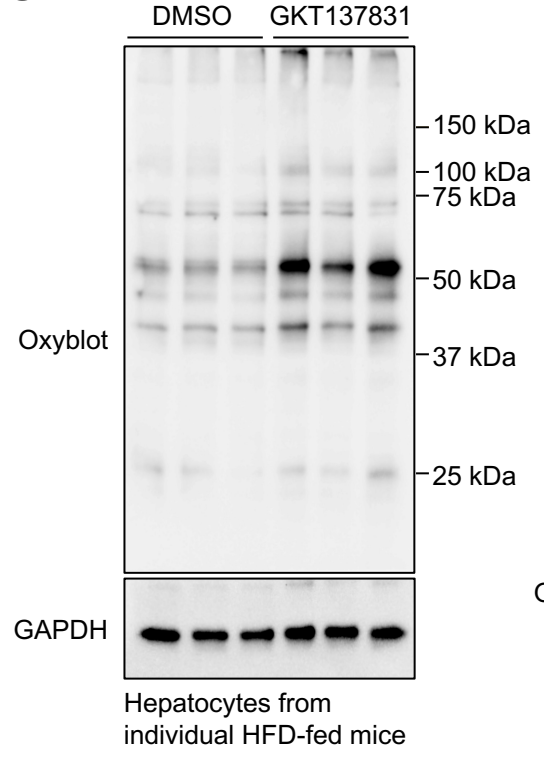
G
DMSO
GKT137831
150 kDa
100 kDa
75 kDa
50 kDa
37 kDa
25 kDa
Oxyblot
GAPDH
Hepatocytes from
individual HFD-fed mice

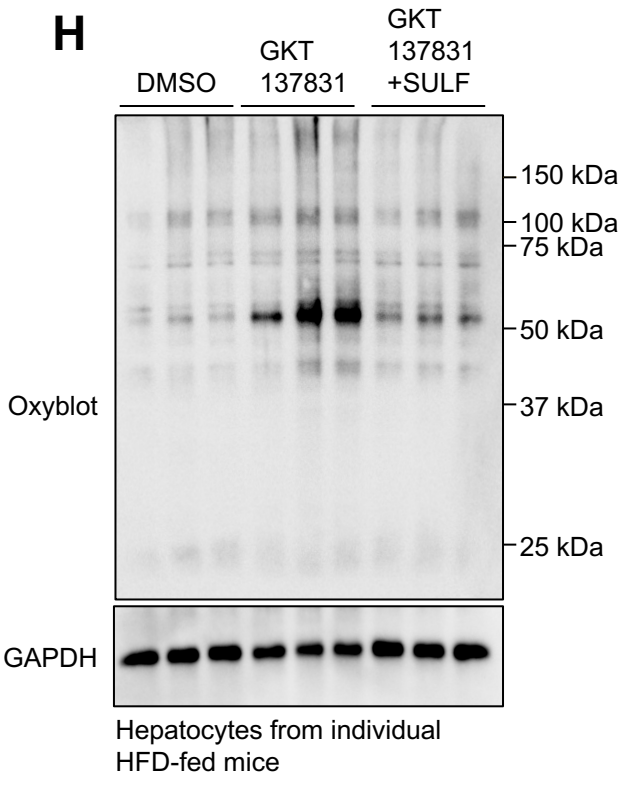
H
DMSO
GKT
137831
GKT
137831
+SULF
150 kDa
100 kDa
75 kDa
50 kDa
37 kDa
25 kDa
Oxyblot
GAPDH
Hepatocytes from individual
HFD-fed mice

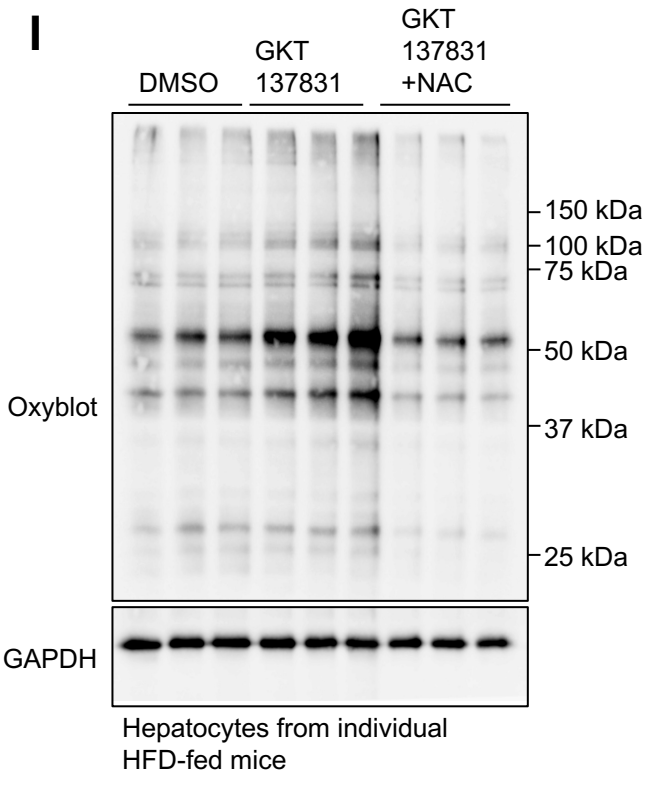
I
DMSO
GKT
137831
GKT
137831
+NAC
150 kDa
100 kDa
75 kDa
50 kDa
37 kDa
25 kDa
Oxyblot
GAPDH
Hepatocytes from individual
HFD-fed mice

FIG 6

Figure 6. NOX4 inhibition diminishes antioxidant defense and promotes oxidative stress and insulin resistance. C57BL/6 mice were fed a HFD for 8-10-weeks and hepatocytes isolated and cultured for 16 h at 5% O_2. **a-b**) Hepatocytes were treated with vehicle (DMSO) or 40 μM GKT137831 twice per day for 48h and processed for **a**) qPCR, or **b**) serum-starved and stimulated with 2 nM insulin and processed for immunoblotting. **c-d**) Hepatocytes were treated with vehicle, GKT137831 twice per day, or GKT137831 twice per day plus 1 μM SULF once per day for 48h and processed for **c**) qPCR or **d**) immunoblotting. **e-i**) Hepatocytes were treated with DMSO, GKT137831 twice per day or GKT137831 twice per day plus NAC (1 mM) for 48h and then processed for **e**) qPCR, or **f**) stimulated with 2 nM insulin and processed for p-AKT immunoblotting, or **g-i**) processed for Oxyblot immunoblotting. Representative and quantified results are shown (mean±SEM) for the indicated number of mice. Significances were determined using (a) Student's t-test or (c, e) one-way ANOVA; # Student's t-test.

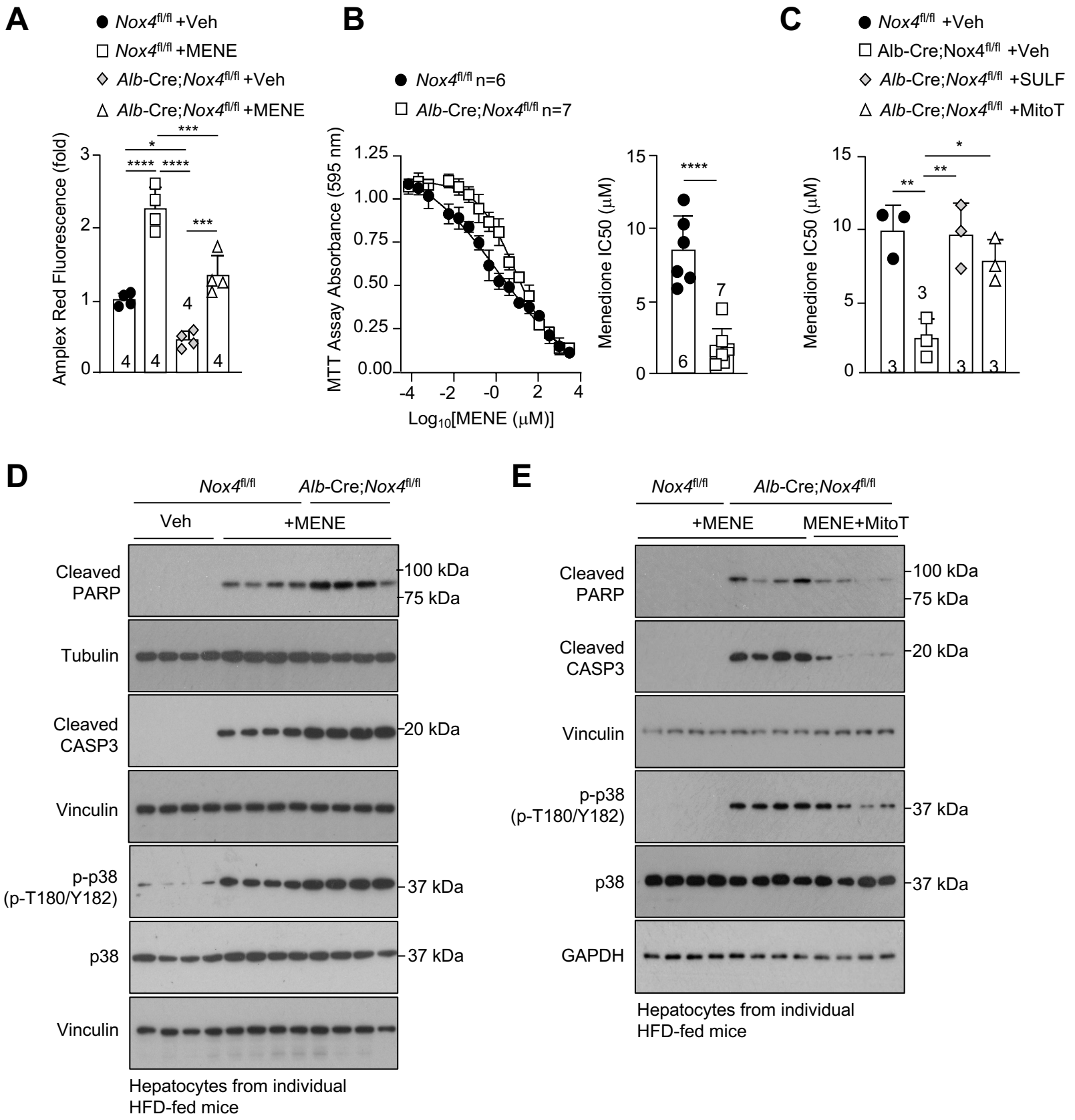
A
Nox4fl/fl +Veh
Nox4fl/fl +MENE
Alb-Cre;Nox4fl/fl +Veh
Alb-Cre;Nox4fl/fl +MENE
Amplex Red Fluorescence (fold)
B
Nox4fl/fl n=6
Alb-Cre;Nox4fl/fl n=7
MTT Assay Absorbance (595 nm)
Log10[MENE (μM)]
Menedione IC50 (μM)
C
Nox4fl/fl +Veh
Alb-Cre;Nox4fl/fl +Veh
Alb-Cre;Nox4fl/fl +SULF
Alb-Cre;Nox4fl/fl +MitoT
Menedione IC50 (μM)
D
Nox4fl/fl
Alb-Cre;Nox4fl/fl
Veh
+MENE
Cleaved PARP
100 kDa
75 kDa
Tubulin
Cleaved CASP3
20 kDa
Vinculin
p-p38 (p-T180/Y182)
37 kDa
p38
37 kDa
Vinculin
Hepatocytes from individual HFD-fed mice
E
Nox4fl/fl
Alb-Cre;Nox4fl/fl
+MENE
MENE+MitoT
Cleaved PARP
100 kDa
75 kDa
Cleaved CASP3
20 kDa
Vinculin
p-p38 (p-T180/Y182)
37 kDa
p38
37 kDa
GAPDH
Hepatocytes from individual HFD-fed mice

FIG 7

Figure 7. Figure 6. NOX4-deficiency promotes cell death. **a-d**) *Nox4*$^{fl/fl}$ or *Alb*-Cre;*Nox4*$^{fl/fl}$ mice were fed a HFD for 8-10-weeks and hepatocytes isolated and **a**) treated with vehicle (EtOH) or 1 μM menadione (MENE) for 16h and processed for H_2O_2 measurements, or **b**) treated with varying concentrations of MENE (16.9μM-3mM) for 48h, or **c**) with vehicle, 1 μM SULF or 20 μM MitoT for 16h and then varying concentrations of MENE for 48h in the presence of 1 μM SULF or 20 μM MitoT as indicated and processed for the analysis of cell death using the MTT assay. **d-e**) Alternatively, cells were incubated with **d**) vehicle or 1 μM MENE for 24h or **e**) with vehicle or 20 μM MitoT for 16h and then 1 μM MENE for 24h in the presence of 20 μM MitoT as indicated and processed for immunoblotting to monitor for cleaved PARP, cleaved caspase 3 (CASP3) and T180/Y182 phosphorylated p38 (p-p38) MAPK. Representative and quantified results are shown (mean±SEM) for the indicated number of mice. Significance determined using (b**)** Student's t-test, or (a, c) two-way ANOVA.

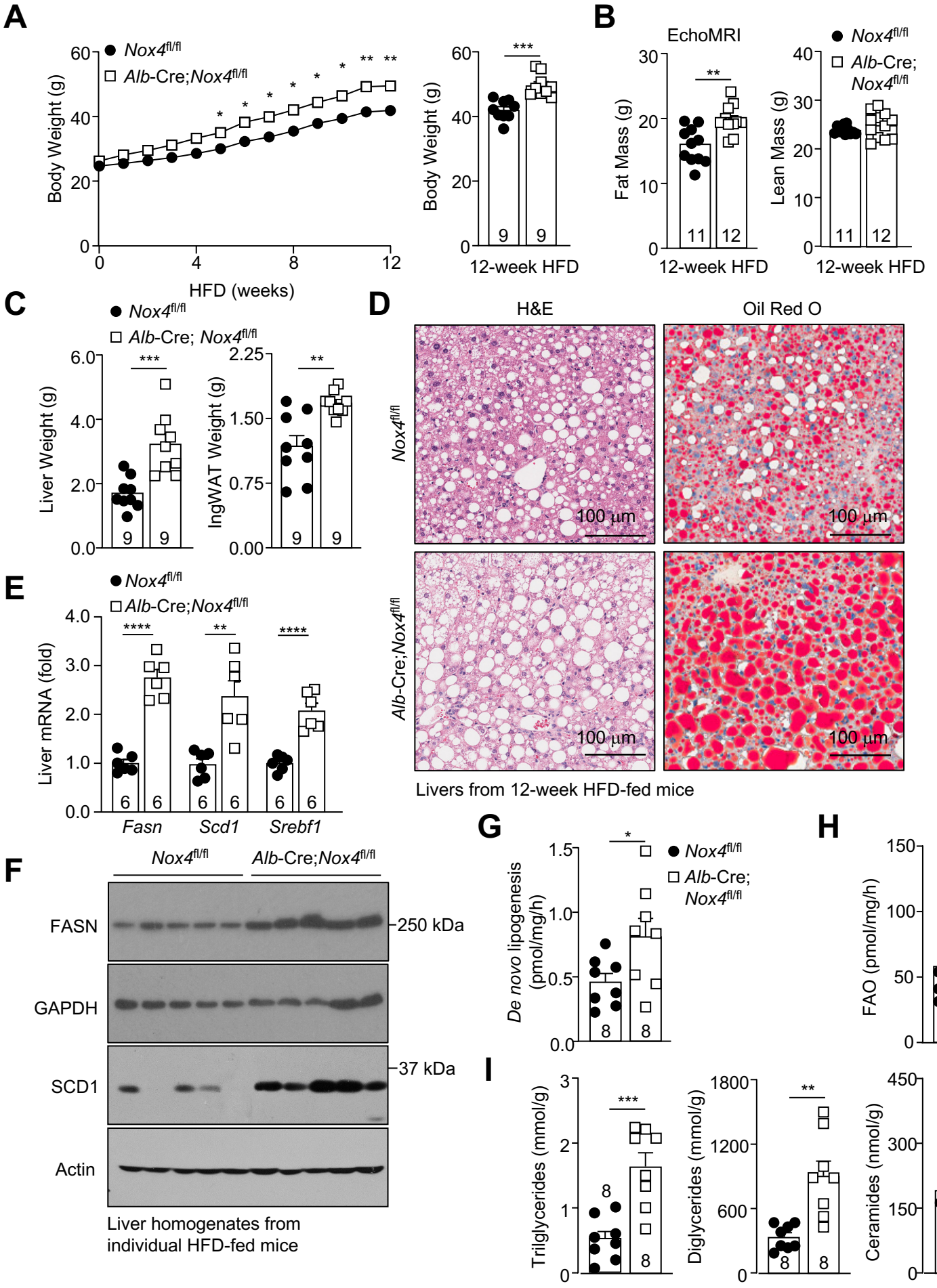
A
Nox4fl/fl
Alb-Cre;Nox4fl/fl
Body Weight (g)
HFD (weeks)
12-week HFD
B
EchoMRI
Fat Mass (g)
Lean Mass (g)
C
Liver Weight (g)
IngWAT Weight (g)
D
H&E
Oil Red O
100 µm
Livers from 12-week HFD-fed mice
E
Liver mRNA (fold)
Fasn
Scd1
Srebf1
F
FASN
GAPDH
SCD1
Actin
250 kDa
37 kDa
Liver homogenates from individual HFD-fed mice
G
De novo lipogenesis (pmol/mg/h)
H
FAO (pmol/mg/h)
I
Triglycerides (mmol/g)
Diglycerides (mmol/g)
Ceramides (nmol/g)

FIG 8

Figure 8. NOX4-deficiency promotes obesity, steatosis and insulin resistance. *Nox4*$^{fl/fl}$ and *Alb*-Cre;*Nox4*$^{fl/fl}$ male mice were fed a HFD for 12-weeks. **a**) Body weights, **b**) body composition, **c**) liver and inguinal white adipose tissue (ingWAT) weights. **d**) Livers were processed for histology (H&E: hematoxylin and eosin or Oil Red O). **e-i**) Livers were processed for **e**) qPCR, or **f**) immunoblotting, or biochemical assays to measure **g**) *de novo* lipogenesis, **h**) fatty acid oxidation (FAO) as well as **i**) triglyceride, diglyceride and ceramide levels. Representative and quantified results are shown (means±SEM) for the indicated number of mice; significance determined using (a) two-way ANOVA, (a) Student's t-test (12-week body weight) or (b-c, e, g-i) Student's t-test.

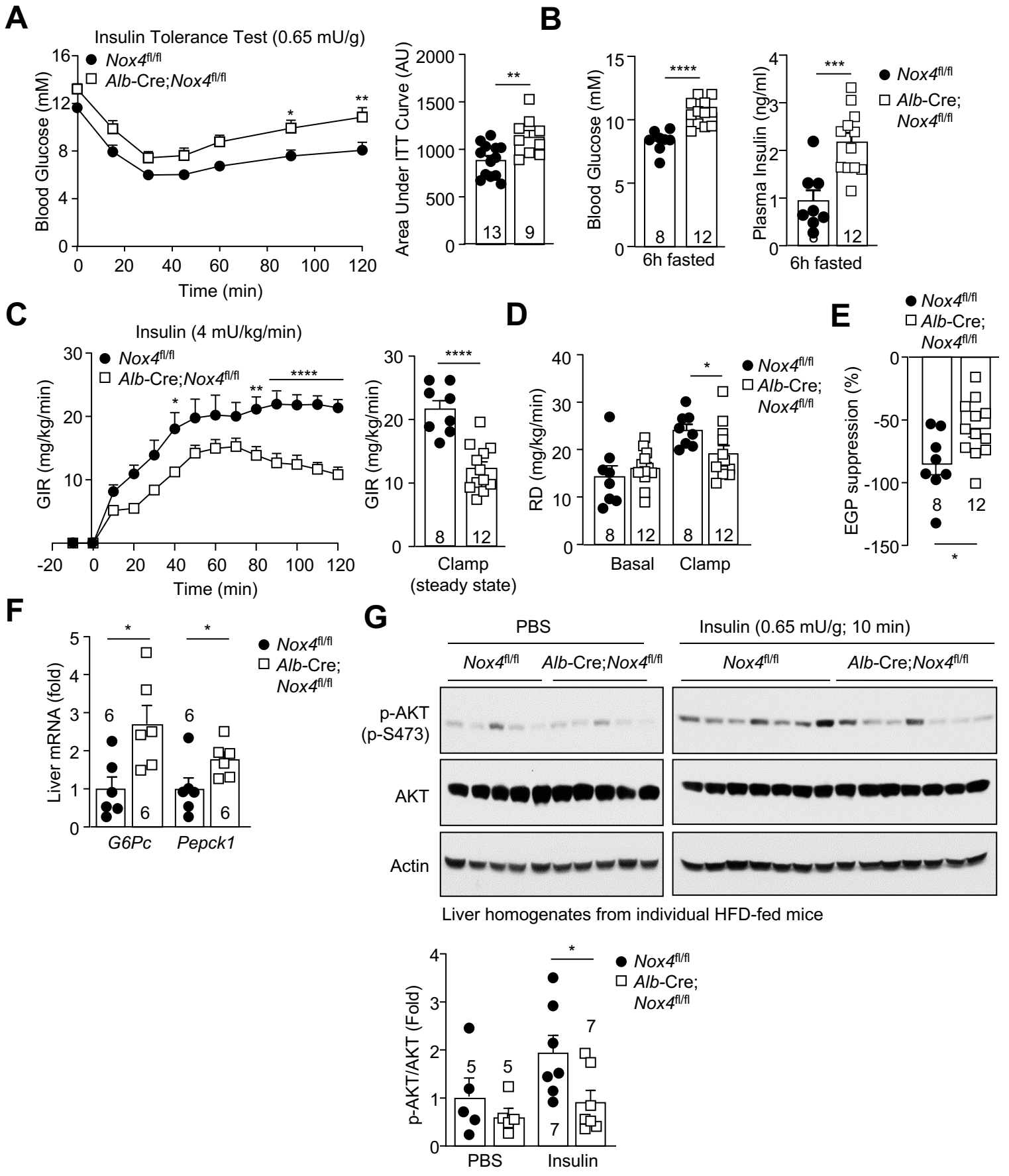
A
Insulin Tolerance Test (0.65 mU/g)
Nox4fl/fl
Alb-Cre;Nox4fl/fl
Blood Glucose (mM)
Time (min)
Area Under ITT Curve (AU)
B
Blood Glucose (mM)
6h fasted
Plasma Insulin (ng/ml)
6h fasted
C
Insulin (4 mU/kg/min)
GIR (mg/kg/min)
Time (min)
Clamp
(steady state)
D
RD (mg/kg/min)
Basal
Clamp
E
EGP suppression (%)
F
Liver mRNA (fold)
G6Pc
Pepck1
G
PBS
Insulin (0.65 mU/g; 10 min)
p-AKT
(p-S473)
AKT
Actin
Liver homogenates from individual HFD-fed mice
p-AKT/AKT (Fold)
PBS
Insulin

FIG 9

Figure 9. NOX4-deficiency promotes insulin resistance. **a-g**) *Nox4*$^{fl/fl}$ and *Alb*-Cre;*Nox4*$^{fl/fl}$ male mice were fed a HFD for 12-weeks. **a**) Mice were subjected to insulin tolerance tests [ITTs; areas under ITT curves determined; arbitrary units (AU) shown], or fasted for 6h and **b**) blood glucose and plasma insulin levels determined, or subjected to hyperinsulinaemic-euglycaemic clamps. **c**) GIRs and **d**) RD **e**) EGP (% suppression). **f**) Clamped livers were processed for qPCR. **g**) Mice were fasted for 6h, injected with PBS or insulin and livers processed for immunoblotting. Representative and quantified results are shown (means±SEM) for the indicated number of mice; significance determined using (a b, c, d, e-g) Student's t-test, or (a, c) two-way ANOVA (ITT curves and GIR time courses).

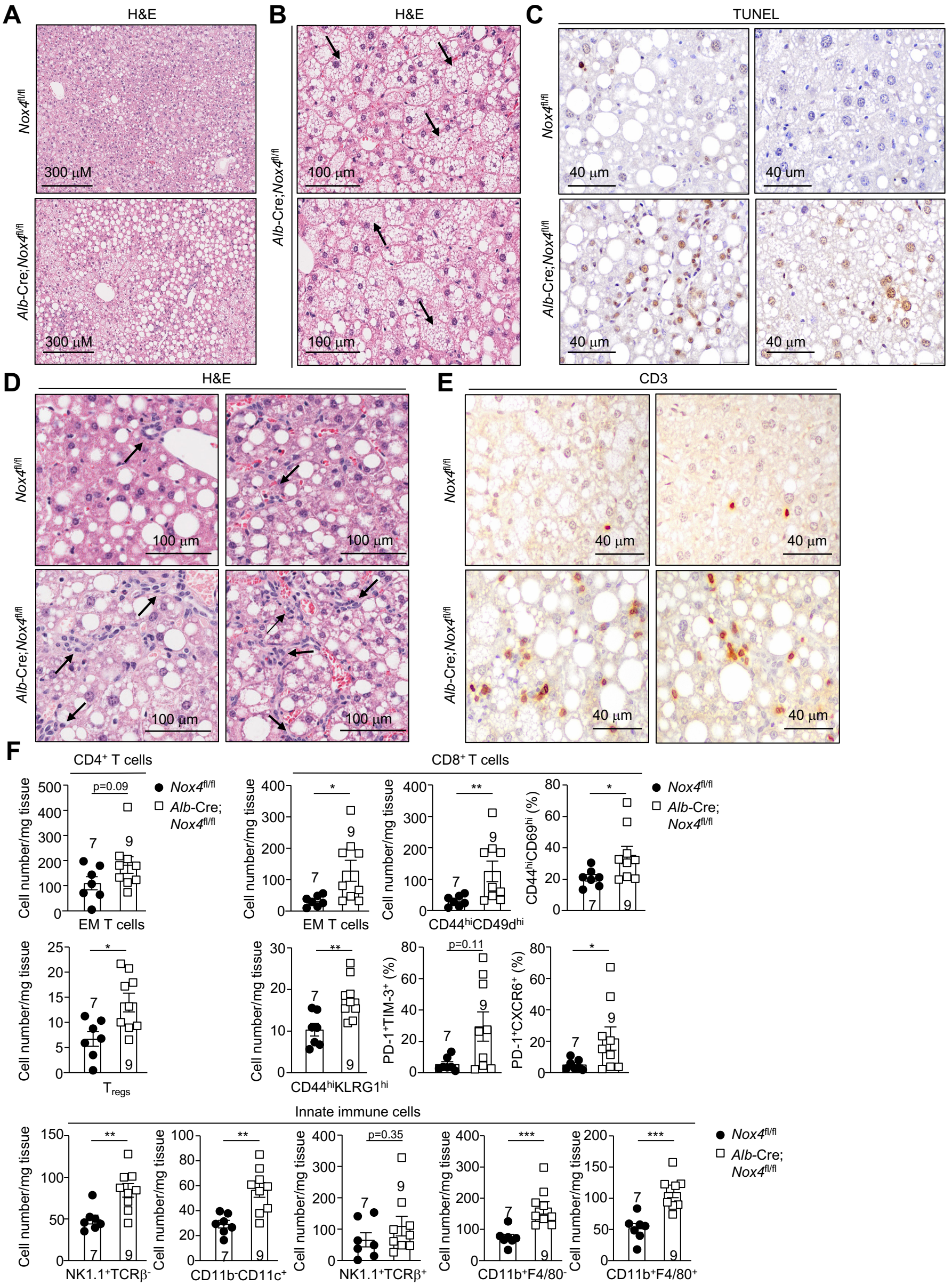
A
H&E
Nox4fl/fl
Alb-Cre;Nox4fl/fl
300 μM
B
H&E
Alb-Cre;Nox4fl/fl
100 μm
C
TUNEL
Nox4fl/fl
Alb-Cre;Nox4fl/fl
40 μm
D
H&E
Nox4fl/fl
Alb-Cre;Nox4fl/fl
100 μm
E
CD3
Nox4fl/fl
Alb-Cre;Nox4fl/fl
40 μm
F
CD4+ T cells
CD8+ T cells
Nox4fl/fl
Alb-Cre; Nox4fl/fl
Cell number/mg tissue
p=0.09
EM T cells
CD44hiCD49dhi
CD44hiCD69hi (%)
Tregs
CD44hiKLRG1hi
PD-1+TIM-3+ (%)
p=0.11
PD-1+CXCR6+ (%)
Innate immune cells
NK1.1+TCRβ-
CD11b-CD11c+
NK1.1+TCRβ+
CD11b+F4/80-
CD11b+F4/80+
p=0.35

FIG 10

***Figure 10. NOX4-deficiency promotes NASH*. a-h)** *Nox4*$^{fl/fl}$ and *Alb*-Cre;*Nox4*$^{fl/fl}$ male mice were fed a HFD for 12-weeks. **a-e**) Livers were processed either for **a-b, d**) histology (H&E) to monitor **a**) steatosis and **b**) hepatocyte ballooning (indicated by arrows), or **d**) lymphocytic infiltrates (indicated by arrows) or **c**, **e**) immunohistochemistry to monitor for **c**) TUNEL^{+} apoptotic cells or **e**) CD3^{+} T cells. **f**) Liver lymphocytes including CD44^{hi}CD62L^{lo} CD4^{+} and CD8^{+} effector/memory (EM) T cells, CD4^{+}CD25^{+}FoxP3^{+} regulatory T cells (T_{regs}), CD8^{+}CD44^{hi}CD49d^{hi} T cells, CD8^{+}CD44^{hi}CD69d^{hi} T cells, CD8^{+}CD44^{hi}KLRG1^{hi} T cells, CD8^{+}PD-1^{hi}TIM-3^{hi} T cells, CD8^{+}PD-1^{hi}CXCR6^{hi} autoreactive T cells, NK1.1^{hi}TCRβ^{lo} natural killer (NK) cells, NK1.1^{hi}TCRβ^{hi} NK T cells, CD11b^{-}CD11c^{+} lymphoid dendritic cells, CD11b^{hi}F4/80^{lo} hepatic macrophages and CD11b^{hi}F4/80^{hi} Kupffer cells were analysed by flow cytometry. Representative and quantified results are shown (means±SEM) for the indicated number of mice; significance in (f) was determined using a 2-tailed Mann-Whitney U Test.

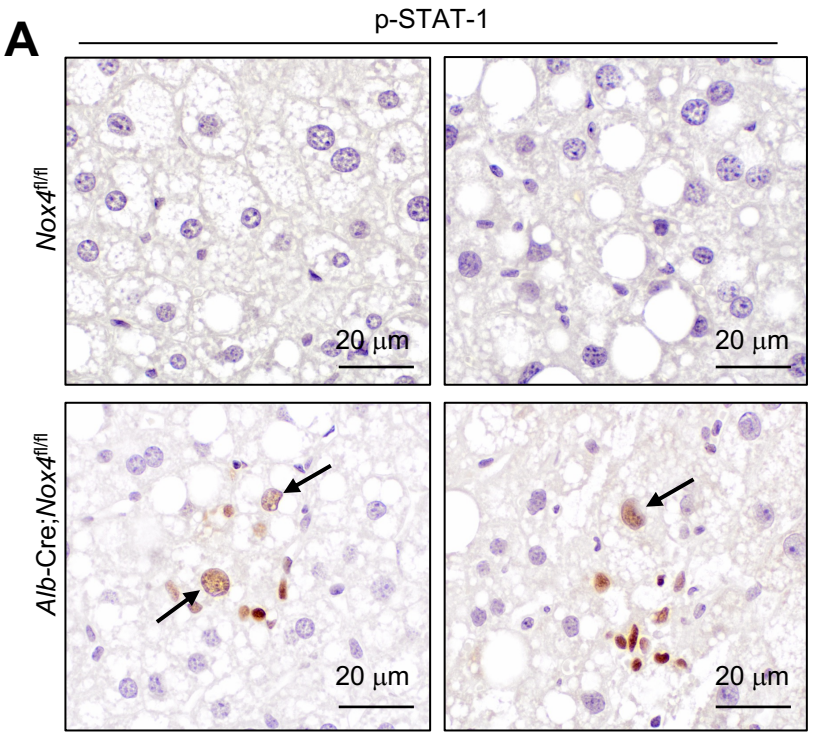
A
p-STAT-1
Nox4fl/fl
Alb-Cre;Nox4fl/fl
20 μm

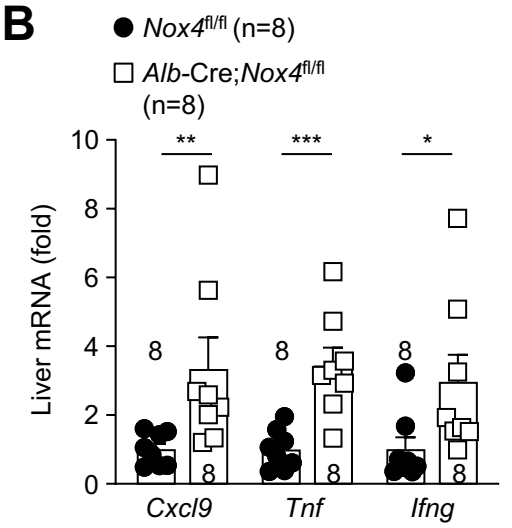
B
Nox4fl/fl (n=8)
Alb-Cre;Nox4fl/fl (n=8)
Liver mRNA (fold)
Cxcl9
Tnf
Ifng
**
***
*

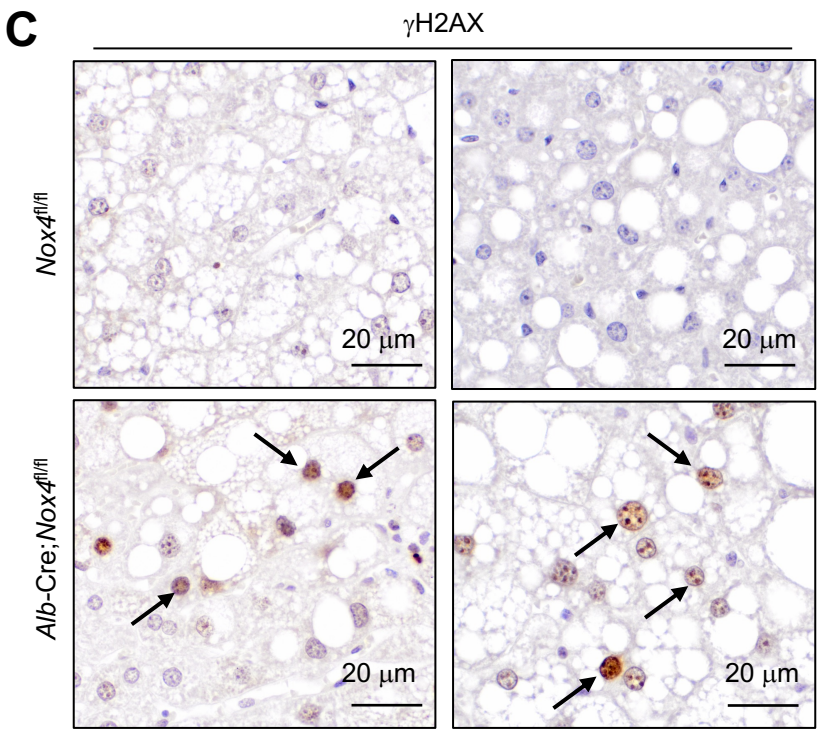
C
γH2AX
Nox4fl/fl
Alb-Cre;Nox4fl/fl
20 μm

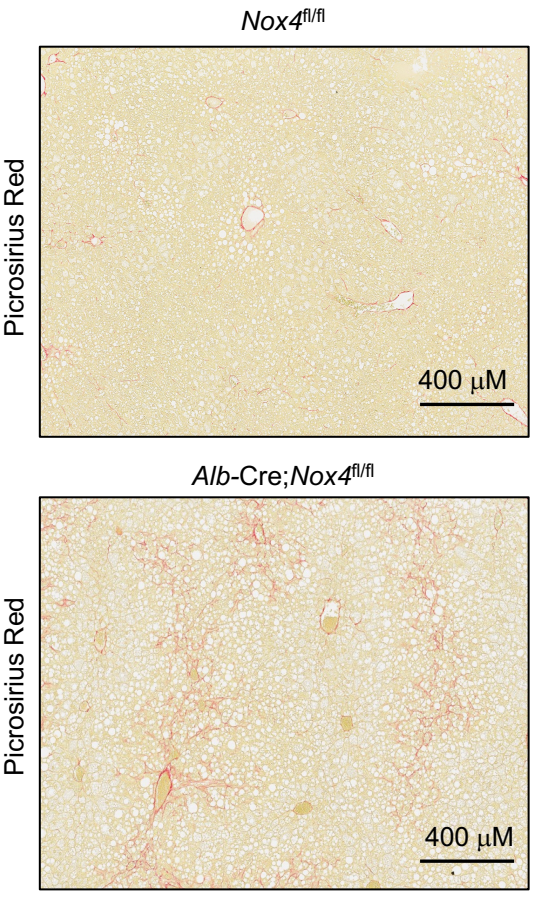
D
Nox4fl/fl
Alb-Cre;Nox4fl/fl
Picrosirius Red
400 μM

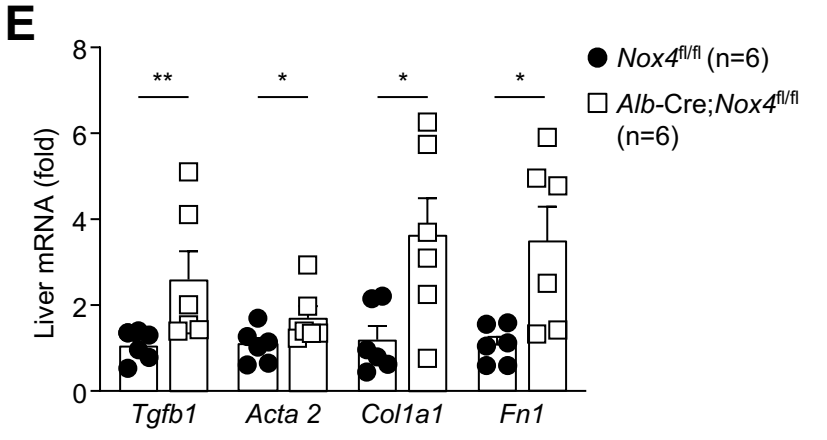
E
Liver mRNA (fold)
Nox4fl/fl (n=6)
Alb-Cre;Nox4fl/fl (n=6)
Tgfb1
Acta 2
Col1a1
Fn1
**
*

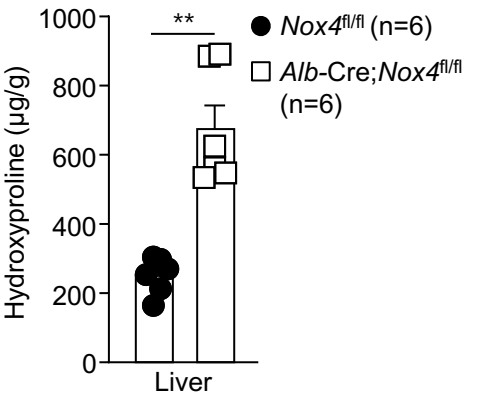
F
Hydroxyproline (μg/g)
Nox4fl/fl (n=6)
Alb-Cre;Nox4fl/fl (n=6)
Liver
**

FIG 11

Figure 11. NOX4-deficiency promotes inflammation and fibrosis. **a-f)** *Nox4*$^{fl/fl}$ and *Alb*-Cre;*Nox4*$^{fl/fl}$ male mice were fed a HFD for 12-weeks. **a**) Livers were processed for immunohistochemistry to monitor for STAT-1 Y701 phosphorylation (p-STAT-1; p-STAT-1+ hepatocytes indicated by arrows). **b**) Liver *Cxcl9*, *Tnf* and *Ifng* mRNA levels were assessed by qPCR. **c**) Livers were processed for immunohistochemistry to monitor for DNA damage (γH2AX+ hepatocytes indicated by arrows). **d**) Livers were processed for PicroSirius Red staining to monitor for fibrosis. **e**) Liver *Acta2, Tgfb*, *Col1a1* and *Fn1* mRNA levels were assessed by qPCR. **f**) Liver hydroxyproline levels. Representative and quantified results are shown (means±SEM) for the indicated number of mice; significance (b, e, f) determined using Student's t-tests.

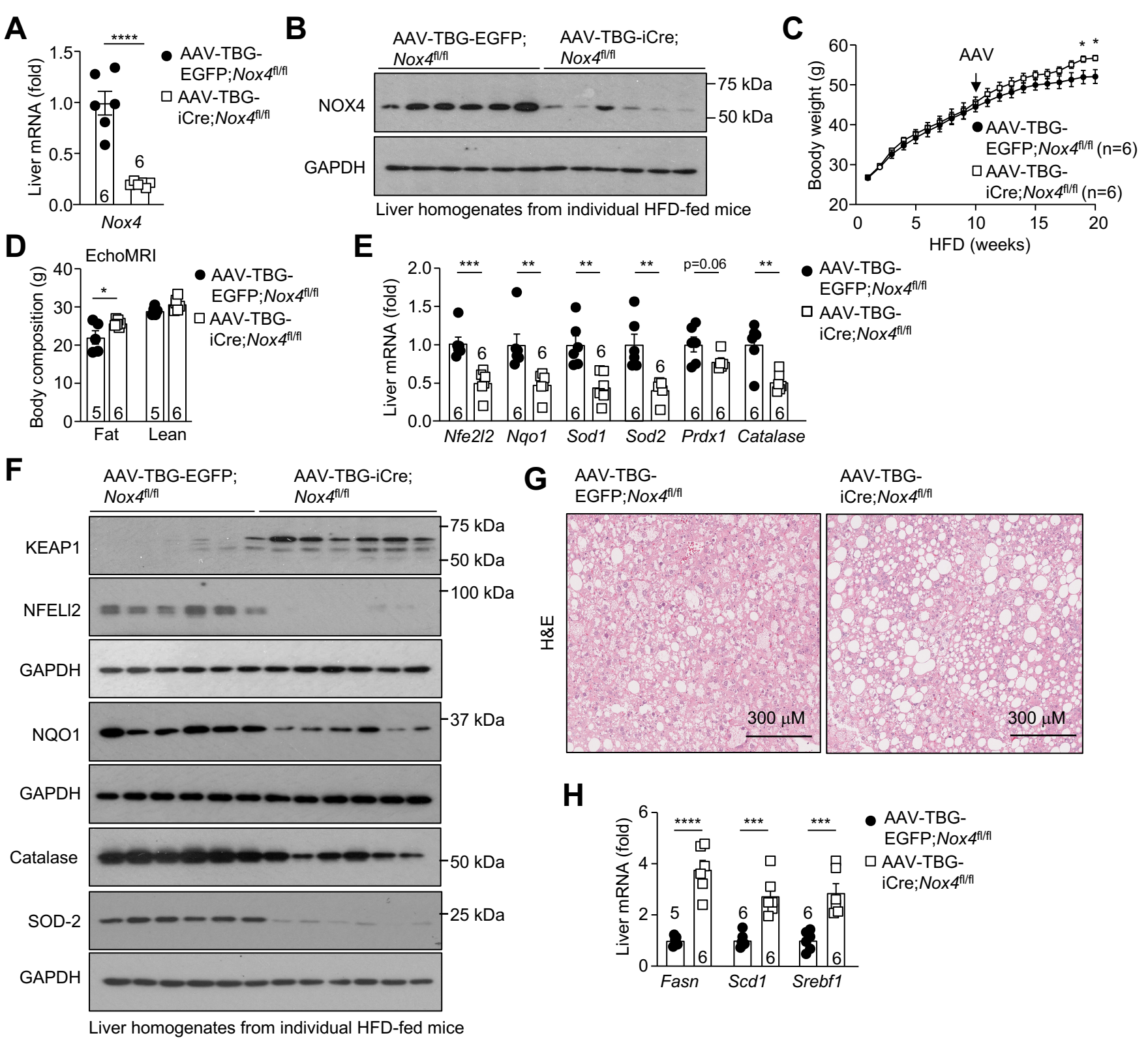
A
Liver mRNA (fold)
****
AAV-TBG-EGFP;Nox4fl/fl
AAV-TBG-iCre;Nox4fl/fl
Nox4
B
AAV-TBG-EGFP; Nox4fl/fl
AAV-TBG-iCre; Nox4fl/fl
NOX4
GAPDH
75 kDa
50 kDa
Liver homogenates from individual HFD-fed mice
C
Boody weight (g)
AAV
HFD (weeks)
AAV-TBG-EGFP;Nox4fl/fl (n=6)
AAV-TBG-iCre;Nox4fl/fl (n=6)
D
EchoMRI
Body composition (g)
Fat
Lean
E
Liver mRNA (fold)
p=0.06
Nfe2l2
Nqo1
Sod1
Sod2
Prdx1
Catalase
F
KEAP1
NFELI2
GAPDH
NQO1
37 kDa
SOD-2
25 kDa
G
H&E
300 μM
H
Fasn
Scd1
Srebf1

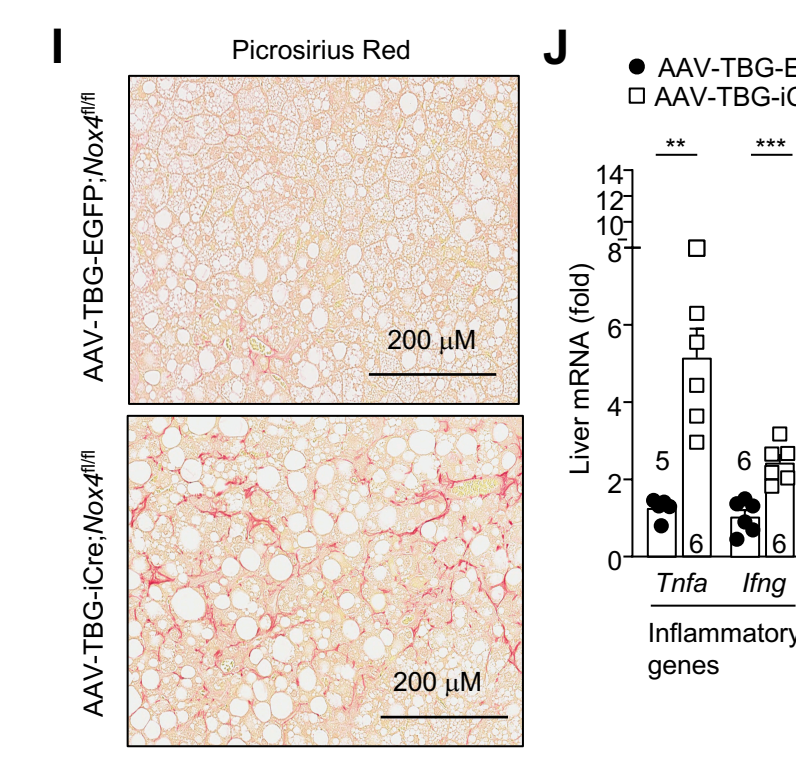
Catalase
50 kDa
SOD-2
25 kDa
GAPDH
Liver homogenates from individual HFD-fed mice

I
Picrosirius Red
AAV-TBG-EGFP;Nox4fl/fl
AAV-TBG-iCre;Nox4fl/fl
200 μM
J
Liver mRNA (fold)
p=0.076
Tnfa
Ifng
Tgfb
Acta2
Col1a1
Fn1
Inflammatory genes
Fibrotic genes
K
Hydroxyproline (μg/g)
Liver

FIG 12

***Figure 12. NOX4-deficiency in obese adult mice promotes NASH/fibrosis*. a-i**) Male *Nox4*$^{fl/fl}$ mice fed a HFD for 10-weeks were administered (intravenous) AAV-TBG-iCre or AAV-TBG-EGFP and then HFD-fed for a further 10-weeks. Livers were processed for **a**) qPCR or **b**) immunoblotting. **c**) Body weights and **d**) body composition. Livers were processed for **e**) qPCR or **f**) immunoblotting to monitor for antioxidant defense, **g**) histology (H&E) and **h**) qPCR to monitor for steatosis, and **i**) histology (Picrosirius Red) and **j**) qPCR to monitor for fibrosis and inflammation. **k**) Liver hydroxyproline levels. Representative results (means±SEM) from at least two independent experiments are shown. Significance in (a, c-e, h, j-k) determined using Student's t-tests.

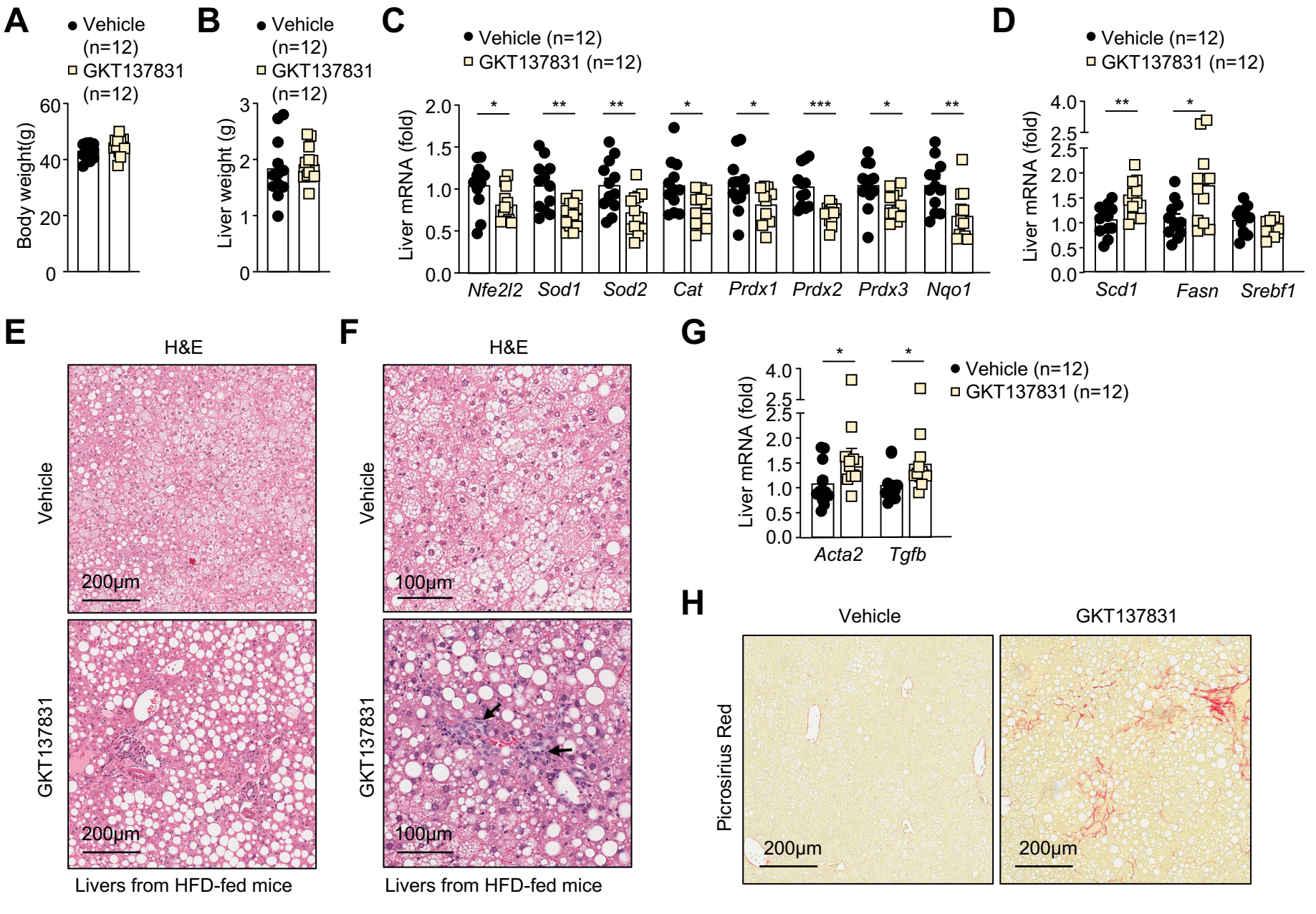
A
Vehicle (n=12)
GKT137831 (n=12)
Body weight(g)
B
Liver weight (g)
C
Liver mRNA (fold)
Nfe2l2
Sod1
Sod2
Cat
Prdx1
Prdx2
Prdx3
Nqo1
D
Scd1
Fasn
Srebf1
E
H&E
Vehicle
GKT137831
200μm
Livers from HFD-fed mice
F
100μm
G
Acta2
Tgfb
H
Picrosirius Red

FIG 13

Figure 13. NOX4 inhibition promotes NASH/fibrosis in HFD-fed mice. **a-f)** C57BL/6 male mice were fed a HFD for 15-weeks and administered GKT137831 (40 mg/kg, 3x/week, oral gavage) for 5 weeks. **a**) Body weights. **b**) Liver weights. Livers were processed for **c-d**) qPCR to assess the expression of **c**) antioxidant defense s or **d**) lipogenic genes. Livers were processed for **e-f**) H&E staining to monitor for **e**) steatosis, or **f**) lymphocytic infiltrates (indicated by arrows). Livers were processed for **g**) qPCR to assess the expression of fibrosis-related genes, or **h**) or histology (PicroSirius Red). Representative and quantified results are shown (means±SEM) for the indicated number of mice. Significance in (a-d, g) was determined using Student's t-test.

A

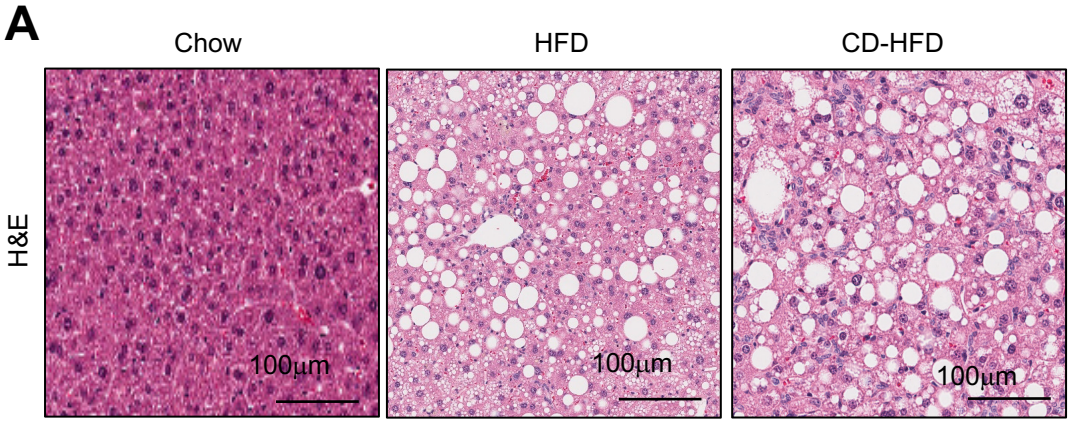

B

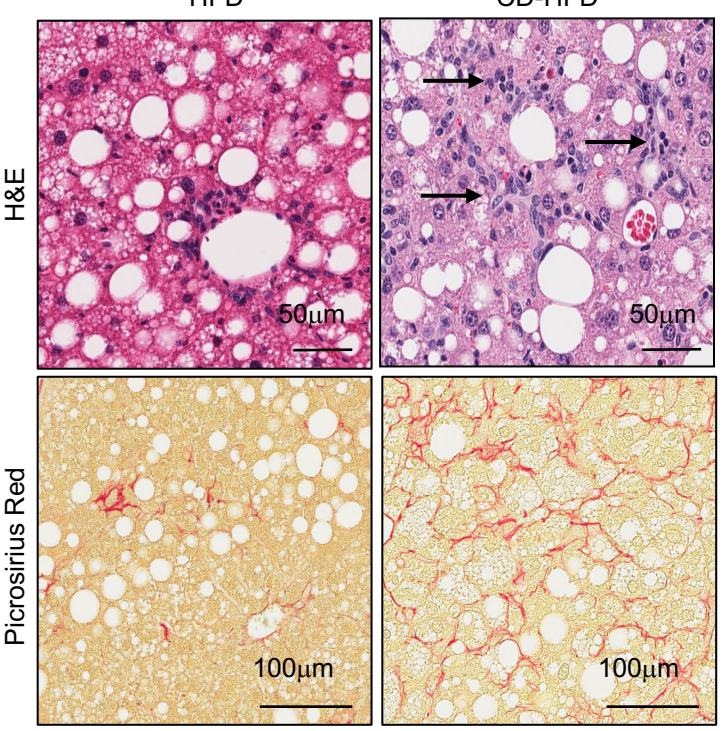

C

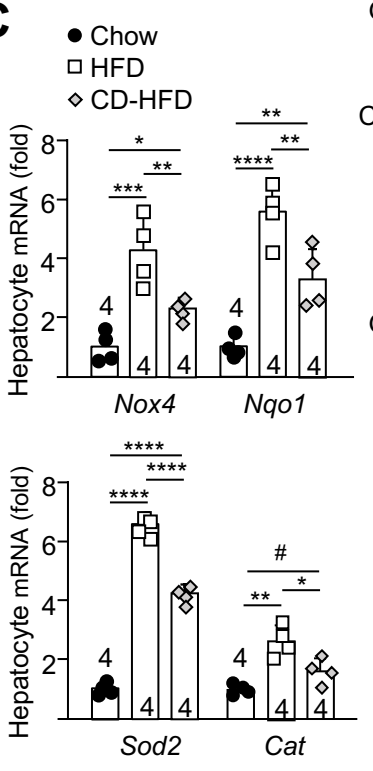

D

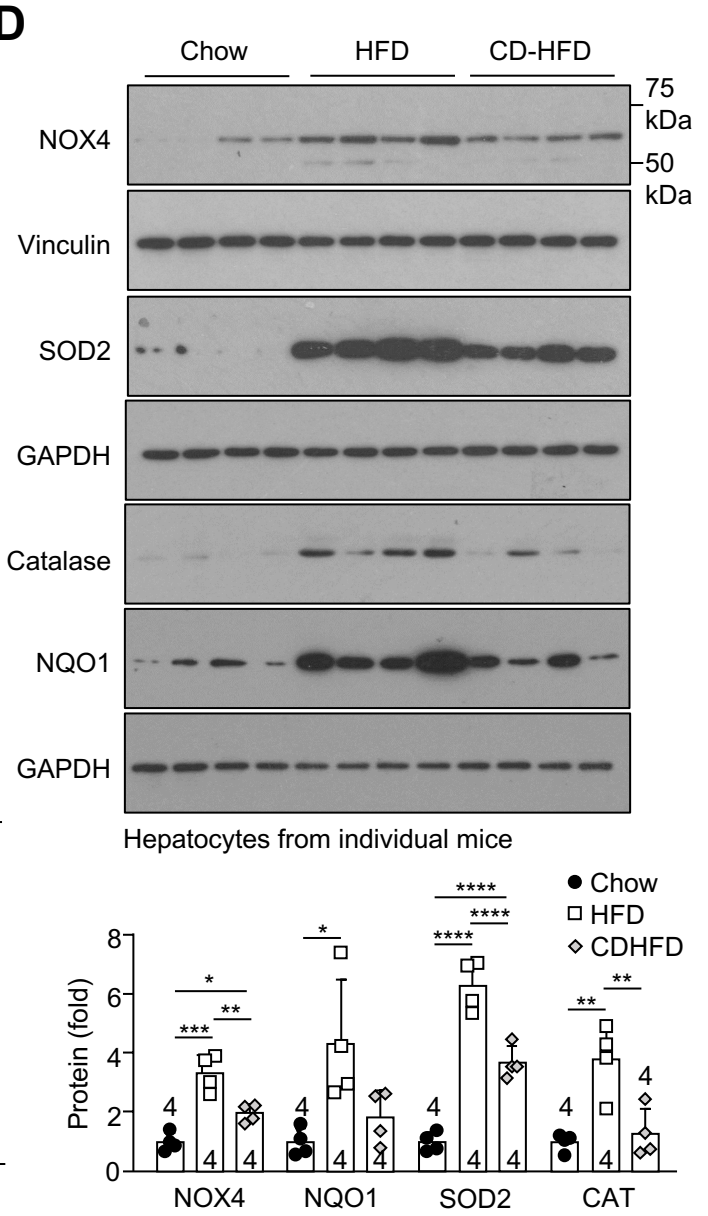

E

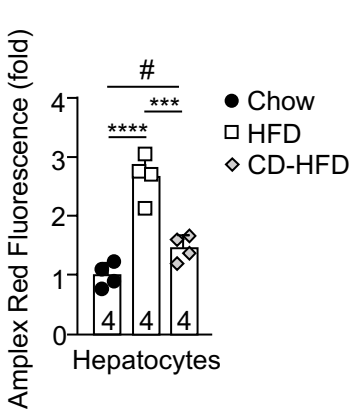

F

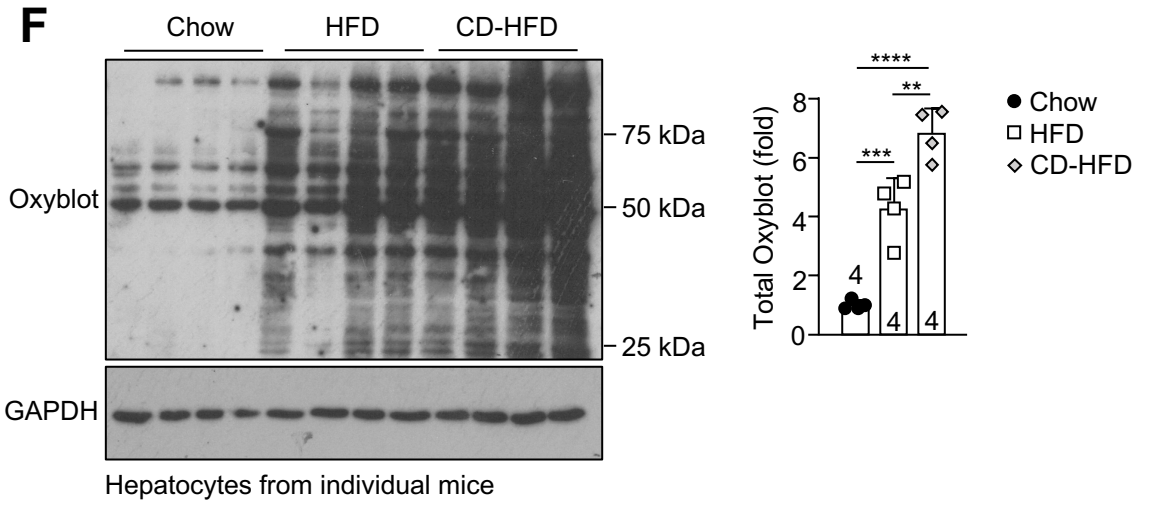

G

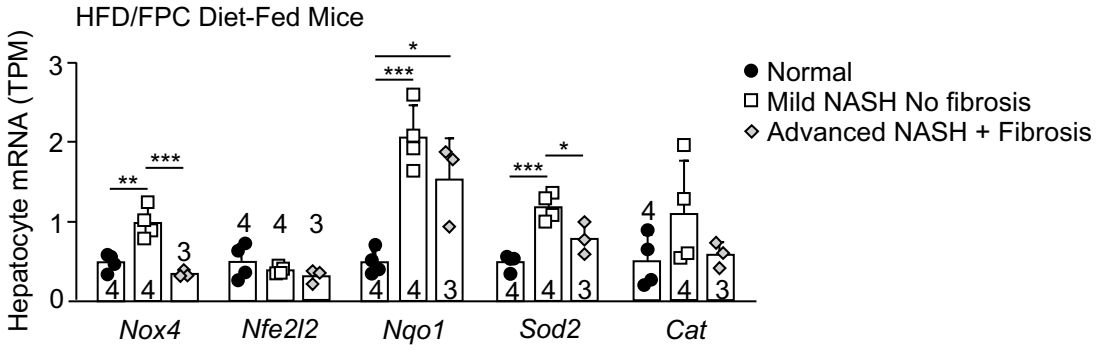

FIG 14

Figure 14. Reduced NOX4 and antioxidant defense gene expression in NASH with advanced fibrosis. **a-f)** C57BL/6 male mice were fed a chow-diet, a HFD or a CD-HFD for 12-weeks. Livers were processed for histology **a**) and stained with H&E to monitor for steatosis, **b)** or lymphocytic infiltrates (indicated by arrows), or stained with Picrosirius Red to monitor for fibrosis. **c-f**) Hepatocytes were isolated and processed for **c)** qPCR, **d)** immunoblotting, **e)** H_2O_2 measurements, or **f**) protein carbonylation analysis. **g**) RNAseq analysis (GSE162876) of hepatocyte nuclei from HEP-INTACT mice (59) fed a low-fat control diet (n=4) versus a HFD rich in fructose, palmitate and cholesterol (HFD/FPC diet) for 20-weeks; HFD/FPC diet-fed mice stratified into those with, mild fibrosis (n=4) or overt inflammation and advanced fibrosis (n=3). Representative and quantified results are shown (mean±SEM) for the indicated number of mice. Significance (c, d, e, f, g) determined using one-way ANOVA; # Student's t-test.

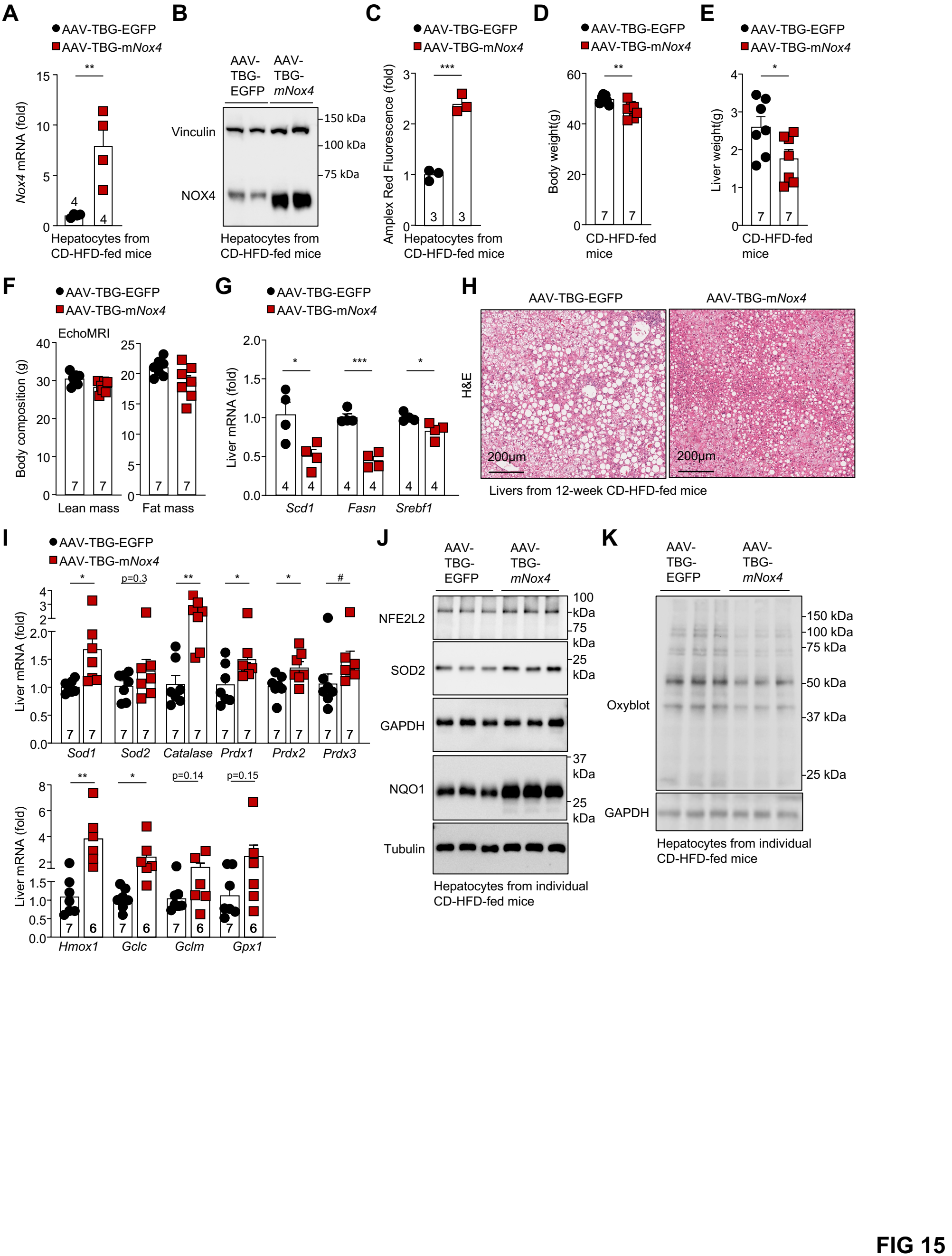
A
AAV-TBG-EGFP
AAV-TBG-mNox4
Nox4 mRNA (fold)
Hepatocytes from CD-HFD-fed mice
B
AAV-TBG-EGFP
AAV-TBG-mNox4
Vinculin
NOX4
150 kDa
100 kDa
75 kDa
Hepatocytes from CD-HFD-fed mice
C
Amplex Red Fluorescence (fold)
Hepatocytes from CD-HFD-fed mice
D
Body weight(g)
CD-HFD-fed mice
E
Liver weight(g)
CD-HFD-fed mice
F
EchoMRI
Body composition (g)
Lean mass
Fat mass
G
Liver mRNA (fold)
Scd1
Fasn
Srebf1
H
H&E
Livers from 12-week CD-HFD-fed mice
I
Liver mRNA (fold)
Sod1
Sod2
Catalase
Prdx1
Prdx2
Prdx3
Hmox1
Gclc
Gclm
Gpx1
p=0.14
p=0.15
J
NFE2L2
SOD2
GAPDH
NQO1
Tubulin
Hepatocytes from individual CD-HFD-fed mice
K
Oxyblot
GAPDH
Hepatocytes from individual CD-HFD-fed mice

FIG 15

Figure 15. NOX4 overexpression promotes antioxidant defense and tempers steatosis and oxidative damage. C57BL/6 male mice were administered (intravenous) AAV-TBG-EGFP or AAV-TBG-m*Nox4* and fed a CD-HFD for up to 12-weeks. **a-c**) Hepatocytes were isolated and processed for **a**) qPCR, **b**) immunoblotting, or **c**) extracellular H_2O_2 measurements. **d**) Body weights, **e**) liver weights and **f**) body composition in 12-week CD-HFD-fed mice. Livers were processed for **g**) qPCR to assess the expression of lipogenic genes, **h**) histology to monitor for steatosis, or **i**) qPCR to assess antioxidant defense gene expression. **j-k**) Hepatocytes were isolated and **j**) the abundance of antioxidant defenses proteins and **k**) protein carbonylation (Oxyblot) assessed by immunoblotting. Representative and quantified results are shown (mean±SEM) for the indicated number of mice. Significance (c-e, g, i) determined using Student's t-test. # significance using 2-tailed Mann-Whitney U Test.

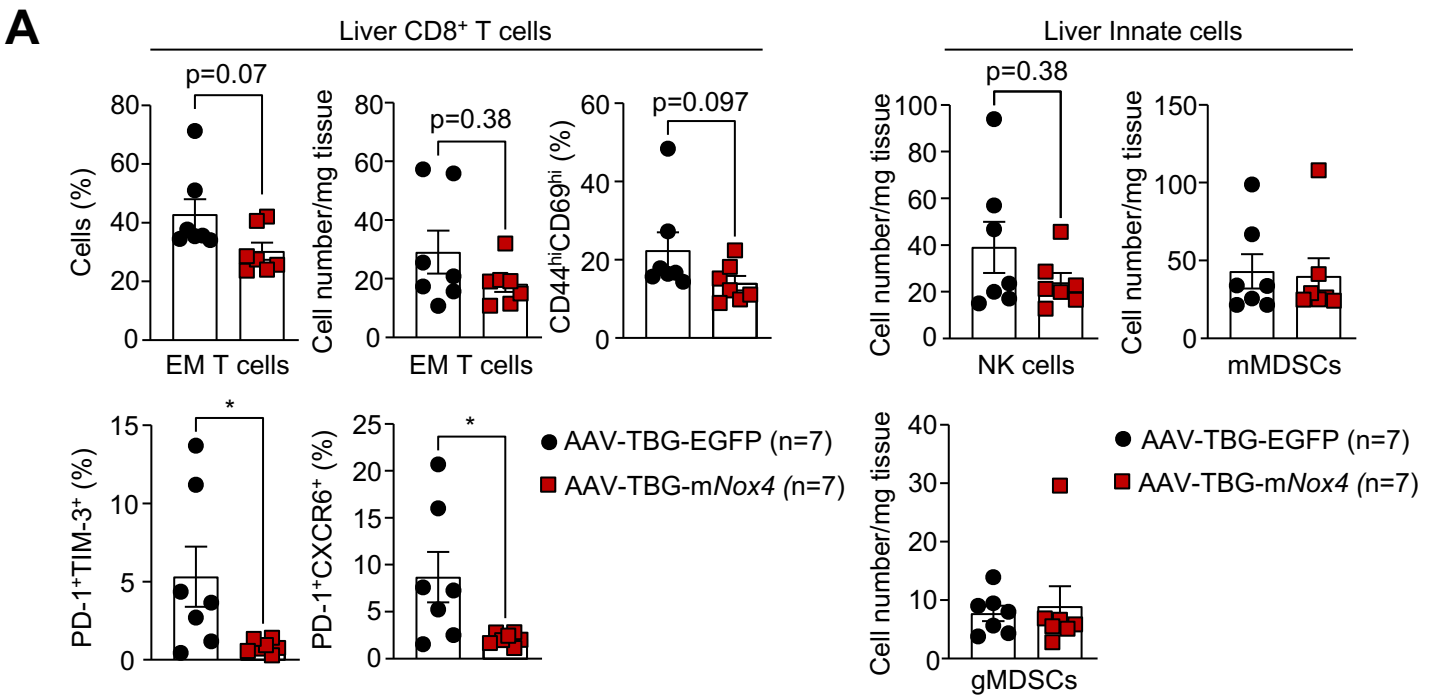

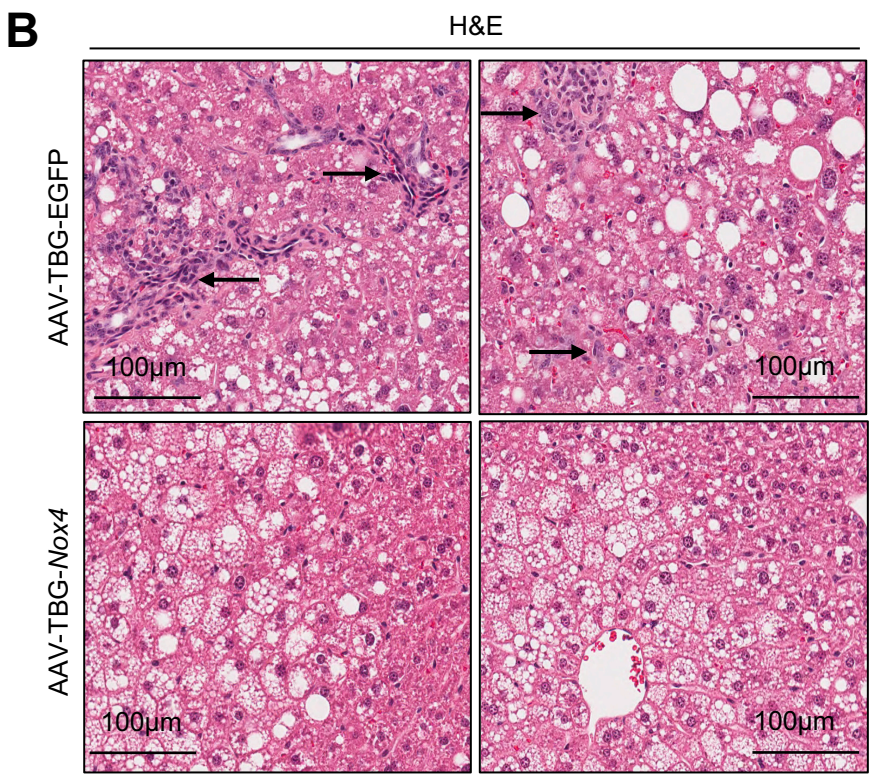

Livers from 12-week CD-HFD-fed mice

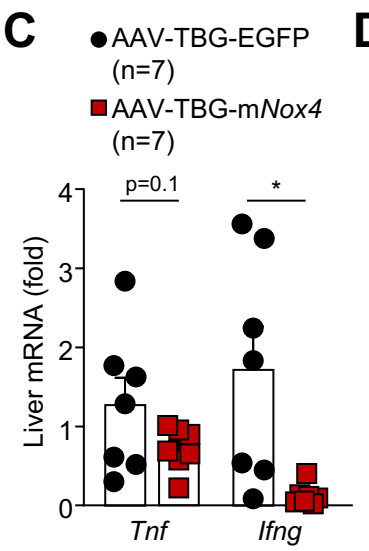

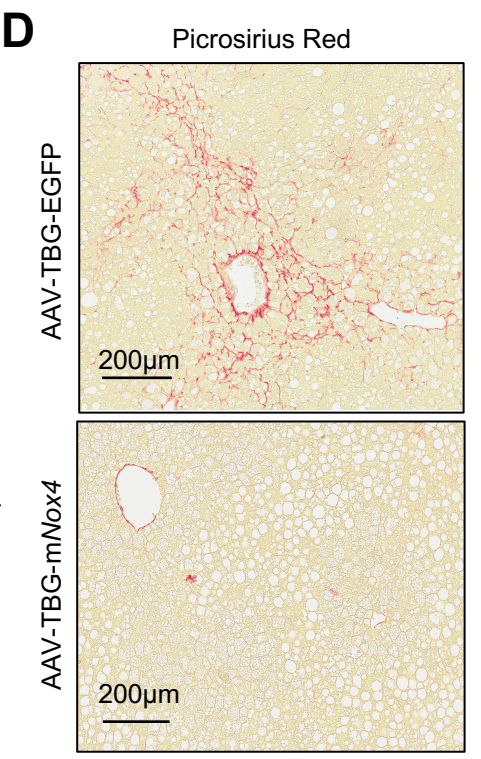

Livers from 12-week CD-HFD-fed mice

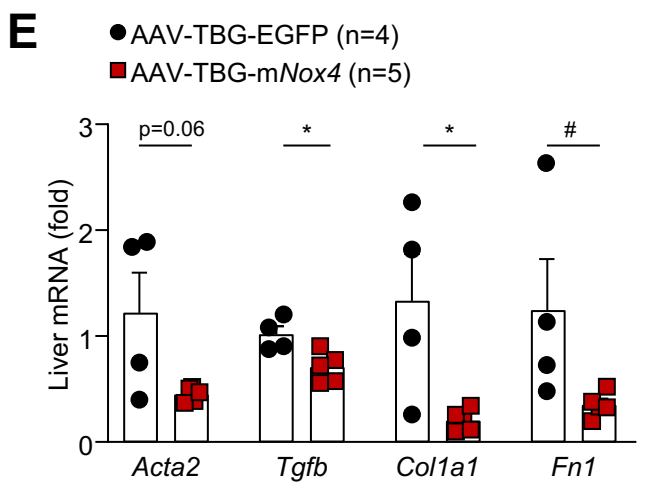

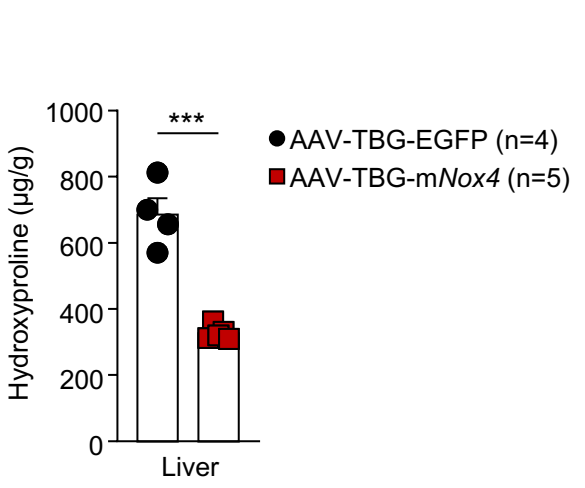

FIG 16

Figure 16. NOX4 overexpression tempers NASH/fibrosis. C57BL/6 male mice were administered AAV-TBG-EGFP or AAV-TBG-m*Nox4* and fed a CD-HFD for 12-weeks. **a**) Liver lymphocytes including $CD8^+$ EM T cells, $CD8^+CD44^{hi}CD69^{hi}$ T cells, $CD8^+PD\text{-}1^{hi}TIM\text{-}3^{hi}$ T cells, $CD8^+PD\text{-}1^{hi}CXCR6^{hi}$ autoreactive T cells, NK cells, monocytic myeloid-derived $CD11b^+F4/80^{hi/lo}Ly6C^+Ly6G^-$ (mMDSCs) and granulocytic myeloid-derived $CD11b^+F4/80^{hi/lo}Ly6C^+Ly6G^+$ (gMDSCs) suppressor cells were analysed by flow cytometry. Livers were processed for **b**) histology or **c**) qPCR to monitor for immune cell infiltrates (H&E; lymphocytes indicated by arrows) or inflammation (*Ifng* and *Tnf*). Livers were processed for **d**) histology (Picrosirius Red), **e**) qPCR, or **f**) measurement of hydroxyproline levels to monitor for fibrosis. Representative and quantified results are shown (mean±SEM) for the indicated number of mice. Significance (c, e, f) determined using Student's t-test or (a) a 2-tailed Mann-Whitney U Test.